Detection of Faults and Drifts in the Energy Performance of a Building Using Bayesian Networks

David Bigaud, Abdérafi Charki, Antoine Caucheteux, Fally Titikpina, Téodor Tiplica

J_ID: DS DOI: 10.1115/1.4043922 Date: 6-June-19 Stage: Page: 1 Total Pages: 23

David Bigaud
LARIS (Laboratoire Angevin de Recherche en Ingénierie des Systèmes), University of Angers, 62 Avenue Notre Dame du Lac, Angers 49000, France
e-mail: david.bigaud@univ-angers.fr

Abderafi Charki[1]
LARIS (Laboratoire Angevin de Recherche en Ingénierie des Systèmes), University of Angers, 62 Avenue Notre Dame du Lac, Angers 49000, France
e-mail: abderafi.charki@univ-angers.fr

Antoine Caucheteux
CEREMA (Centre d'Etudes et d'expertise sur les Risques, l'Environnement, la Mobilité et l'Aménagement), 23 Avenue de l'Amiral Chauvin BP 20069, Les Ponts-de-Cé 49136, France
e-mail: antoine.Caucheteux@cerema.fr

Fally Titikpina
LARIS (Laboratoire Angevin de Recherche en Ingénierie des Systèmes), University of Angers, 62 Avenue Notre Dame du Lac, Angers 49000, France
e-mail: fally.titikpina@univ-angers.fr

Teodor Tiplica
LARIS (Laboratoire Angevin de Recherche en Ingénierie des Systèmes), University of Angers, 62 avenue Notre Dame du Lac, Angers 49000, France
e-mail: teodor.tiplica@univ-angers.fr

Detection of Faults and Drifts in the Energy Performance of a Building Using Bayesian Networks

Despite improved commissioning practices, malfunctions or degradation of building systems still contribute to increase up to 20% the energy consumption. During operation and maintenance stage, project and building technical managers need appropriate methods for the detection and diagnosis of faults and drifts of energy performances in order to establish effective preventive maintenance strategies. This paper proposes a hybrid and multilevel fault detections and diagnosis (FDD) tool dedicated to the identification and prioritization of corrective maintenance actions helping to ensure the energy performance of buildings. For this purpose, we use dynamic Bayesian networks (DBN) to monitor the energy consumption and detect malfunctions of building equipment and systems by considering both measured occupancy and the weather conditions (number of persons on site, temperature, relative humidity (RH), etc.). The hybrid FDD approach developed makes possible the use of both measured and simulated data. The training of the Bayesian network for functional operating mode relies on on-site measurements. As far as dysfunctional operating modes are concerned, they rely mainly on knowledge extracted from dynamic thermal analysis simulating various operational faults and drifts. The methodology is applied to a real building and demonstrates the way in which the prioritization of most probable causes can be set for a fault affecting energy performance. The results have been obtained for a variety of simulated situations with faults deliberately injected, such as increase in heating preset temperature and deterioration of the transmission coefficient of the building's glazing. The limitations of the methodology are discussed and are translated in terms of the ability to optimize the experiment design, control period, or threshold adjustment on the control charts used. [DOI: 10.1115/1.4043922]

Keywords: energy performance, fault detection and diagnosis, Bayesian network, weather conditions, occupancy

1 Introduction

According to different sources, it is commonly considered that buildings are responsible for about 30–40% of the energy consumption in Western countries. Many studies have demonstrated that, in the operational and maintenance (O&M) stage, buildings actually use more energy than estimated by energy simulations in the design stage [1]. In Ref. [2], a difference of performance of more than 30% has been estimated. This difference is due to uncertainty in the modeling of energy simulations [3], as well as to differences in occupant behavior and in building use over time (e.g., modifying room functions and building occupancy). Malfunctions/degradation and a bad control of systems also contribute to reduction in comfort and increase in energy consumption (in some cases, 10–20% higher than necessary) [4]. Recently, in Ref. [5], it has been demonstrated that the averaged cooling energy in office buildings was about 16% higher than designed due to operational errors. Even if the efforts are made to improve the continuous commissioning [6], energy consumption is still higher than expected and, therefore, the development of effective preventive maintenance strategies for building systems is very important. Thus, condition-based maintenance plans the maintenance according to the need determined by the system conditions [7]. Nevertheless, despite examples of preventive maintenance for heating, ventilation, air conditioning, and refrigeration [8], automated energy performance diagnosis features are currently scarcely applied in building energy management systems practices. A key-step within the condition-based maintenance process is the ability to monitor the system malfunctioning from the available signals, hereafter referred to as fault detections and diagnosis (FDD). The automated FDD tools are useful to alarm and identify faults promptly and to identify the variables that cause the degradation of performances, with due regard to the level of accepted risk.

Over the last decades, a significant number of researches had been carried out in the developments of FDD methods for building's systems (see, e.g., Ref. [9] for air handling units, [10] for chiller and [11] for HVAC systems). Building energy HVAC FDD has been proved efficient to reduce energy consumption in buildings during O&M stages. Some field observations show that energy savings of 5–30% can be achievable by correcting faults diagnosed in buildings [12]. Recent FDD case studies in Australia [13] show that energy savings between 15% and 28% are possible by implementing HVAC FDD systems. Despite all these benefits,

[1]Corresponding author.

Contributed by the Dynamic Systems Division of ASME for publication in the Journal of Dynamic Systems, Measurement, and Control. Manuscript received February 3, 2018; final manuscript received May 27, 2019; published online xx xx, xxxx. Assoc. Editor: Umesh Vaidya.

FDD tools are still not broadly used in practice due to the time-consuming nature of the tasks (which must be repeated for each building) and to the complexities of FDD algorithms.

According to Ref. [14], FDD methods can be categorized into three types of approaches: quantitative or model-based, qualitative or rule-based, and process-history-based or data-driven.

Quantitative or model-based approaches are usually based on the knowledge of the physical laws describing the system (e.g., heat and mass balances). The common method in the quantitative FDD approach is the residual generation and analysis (difference between measured and simulated values). Model-based approaches do not rely on past data for training; therefore, they are considered efficient for the detection of unknown abnormalities. They can be used at the component as well as the whole building levels.

Qualitative approaches require a prior knowledge of the system from which simplified relationships (e.g., the rule-based method) are developed. This kind of method is rather simple, but it is also specific to the system under study and often requires a "customized" implementation, which mainly relies on experts and developers' knowledge [15].

Process-history-based or data-driven methodologies are also relatively easy to implement, but they require a significant amount of data to be efficient. Since they rely on historical data, one has to study a whole range of various system operations. In addition, they generally cannot be directly applied on another system without taking into account the specificities of the system [16,17]. Process-history-based approaches include methods such as artificial neural network (e.g., Ref. [18]), principal component analysis [19], support vector machine (e.g., Refs. [20] and [21]), Bayesian classifiers (e.g., Ref. [22]), Fisher discriminant analysis (e.g., Ref. [23]), etc.

In Ref. [24], the authors propose to consider a fourth category of approaches: hybrid approaches obtained by connecting several of the aforementioned approaches in order to improve the overall FDD accuracy and robustness. For example, model-based FDD approaches are often connected to data-driven methods. The present research proposes a hybrid approach (data-driven + model-based). Our purpose is to train the FDD tool based on a large data collection and completing knowledge through dynamic energy simulations (DES) in order to study the effect of complementary unobserved/dysfunctional operations.

Bayesian networks (BNs) can be considered as an appropriate method to accurately represent a building, which is considered as a complex system with uncertain, incomplete, and conflicting information. They are deemed a powerful tool to develop expert systems, and they have the potential to detect and diagnose faults or drifts. A BN is a probabilistic graphical model that represents relationships of probabilistic dependence within variables by means of directed acyclic graphs (see Sec. 2). BNs used as a FDD tool offer a number of undeniable advantages: the ability to manipulate continuous and discrete variables, the ability to take into account time through dynamic Bayesian networks (DBNs), object modeling via the formalism of object-oriented Bayesian networks, and the possibility to expand into decision optimization techniques through the use of influence diagrams (extension of Bayesian networks) [25]. Beyond being able to identify the causes of drift or dysfunction, one remarkable aspect of the BNs, that we cannot find in other methods (such as artificial neural network or support vector machine), is the ability to sort them from the most to the least probable and hence to prioritize inspection and maintenance actions. In the frame of research for increasing the energy performances of buildings, BNs have proved their interest and relevancy, for example, for HVAC [26], with focus on chiller [22–27], air-handling units [28,29], and heat pumps' faults diagnosis [30].

In this paper, we develop a generic (in contrast of most other approaches, actually specific) hybrid FDD approach to detect and diagnose drifts in energy consumption in a monitored building instrumented with different sensors. Data are validated and/or completed by means of energy simulations. Expert knowledge enhances the hybrid approach by validating the physical meaning of the architecture of the FDD model. BNs are used here as a generic model to simulate complex inferences—combining influences from weather conditions qualified as external loads (outdoor temperature (OT), relative humidity (RH), wind speed, solar radiation, etc.), variables qualified as internal or intrinsic loads (indoor air temperature, internal sources, rate of infiltration), influences of energy systems behavior (heat or cooling production, regulation, etc.), and the occupants on differing scales of observation (at "office," "floor" or "building" levels)—with regard to the level of energy performance (or consumption) of a building. In practice, the BN-based hybrid FDD approach proposed in this paper can be used either for new projects or for existing buildings for which we aim at enhancing energy efficiency.

The paper is structured as following: in Sec. 2, the general aspects of our hybrid FDD approach based on the principle of Bayesian networks are explained. In Secs. 3 and 4, we present the case study and the application of the hybrid FDD approach to this case. In Sec. 5, we propose a deep discussion on the results and try to show all the abilities of the approach. Finally, we give some conclusions and discuss about future works in Sec. 6.

2 Creation of a Bayesian Network to Monitor the Performance of a Building

2.1 Principle and Properties of Bayesian Networks. A BN is a statistical modeling tool whose formalism makes it possible to deal with uncertainties. The most useful application of BN is to assess hierarchically the possible causes of risks, failures or operational drifts [31]. Today, BN can be considered as a key modeling framework in decision making in a wide variety of domains such as social sciences [32,33], robotics [34,35], biochemistry or biology [36,37], medicine [38,39], engineering [40,41] and, of course, energy.

In order to understand fully the properties of BNs, it must first be clear that they are a hybrid of two different fields: the theory of graphs and the theory of probabilities. In short, a BN is a graphical representation of a probabilistic model revealing the different relationships that the variables of a model can have. It expresses and factorizes the joint probability of m variables in m conditional independences and its structure enables local calculations of probability using all the information about the joint distributions. These conditional independences make it possible to reduce the number of calculations necessary for the inference and learning of a probabilistic model by simply reducing the size of its structure. For example, a joint probability of m variables is written using the chain rule (or "general product" rule) as follows:

$$p(x_1, x_2, \ldots, x_m) = p(x_m|x_{m-1}, \ldots, x_1)\ldots p(x_2|x_1)p(x_1) \quad (1)$$

This equation can be shortened by introducing or defining the conditional independences between its variables. Moreover, by illustrating these independences in the form of a BN, it becomes possible simply to increase the number of conditional probability distributions for each variable in accordance with the parents and rewrite the joint distribution as follows, where $pa(x_i)$ refers to the *pa*rents of x_i:

$$p(x_1, x_2, \ldots, x_m) = \prod_{i=1}^{i=m} p\left(x_i|pa(x_i)\right) \quad (2)$$

Nevertheless, the fact that the conditional distribution for each variable is defined according to its parents does not signify that no other variables influence it. In other words, nodes other than its parents in the BN can influence a node. These nodes are consistent with the Markov condition, which states that a variable is isolated by a subset of variables of the overall set V known as the Markov blanket [42]. A variable is therefore conditionally independent of

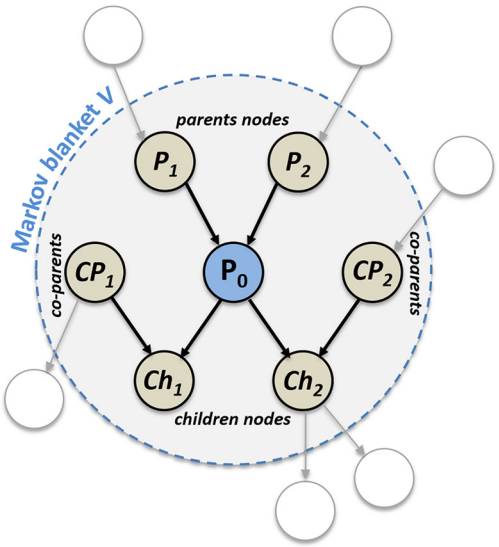

Fig. 1 The Markov Blanket. The shaded nodes (parents, co-parents, children nodes) are inside the Markov Blanket of node "A." The white ones are outside the blanket.

other variables outside its blanket if the nodes of the blanket are observed. This includes its parent and child nodes and the co-parents of its children (see Fig. 1). These nodes, if observed, "block" the node in question from other nodes outside its periphery (see Sec. 4.2 and the discussion related to Fig. 6 for an illustration).

In the example illustrated in Fig. 1, Eq. (2) is developed as

$$\begin{aligned} p(V) &= p(Ch_1, Ch_2, CP_1, CP_2, P_0, P_1, P_2) \\ &= p(P_0|P_1, P_2) \cdot p(Ch_1|CP_1, P_0) \cdot p(Ch_2|CP_2, P_0) \cdot p(P_1) \\ &\quad \cdot p(P_2) \cdot p(CP_1) \cdot p(CP_2) \end{aligned} \tag{3}$$

This property of the BN is not only useful but also essential for inference calculation, and makes it possible to determine instantaneously and visually whether a set of variables is conditionally independent of another one.

The most recent developments in BNs have essentially focused on the inference algorithms [43–45] and on the learning of the structure and parameters of the network [46]. We will concentrate on these aspects in constructing BNs to describe functional and dysfunctional modes in the energy systems of a test building.

2.2 Construction Stages of a Bayesian Network for the Simulation of a Building.

Building management is increasingly relying on automated procedures with sophisticated instrumentation on systems and equipment, allowing the collection of considerable quantities of data. In fact, the volume of data collected is so vast that it would be impossible for an operator to monitor directly each variable involved in the procedure. It seems perfectly logical, therefore, to monitor the technical systems of a building using data-driven methods such as the BN.

The modeling procedure for a building system comprises three stages [47]

- The first stage consists in collecting a database of measured/real inputs (climate, envelope, energy systems, occupants), and outputs (energy needs) calculated from actual data and/or derived from DES. An approach founded entirely on measured inputs and outputs is possible when characterizing an existing building. For a new building, insofar as the energy performance of its equipment and systems cannot be measured on long periods, it is very difficult to characterize the functional and dysfunctional modes. Therefore, the hybrid approach, of real inputs and simulated outputs, proves to be very effective in the majority of situations.
- The second stage consists in learning from the created database to construct a BN (i.e., to model casual relationships and conditional probability distributions between the variables that will influence the energy performance) enables to mimic the building and its energy systems in their normal operational modes. That is to establish a "baseline," essentially, from which to observe operational drifts. This stage is regarded as the inductive part of the BN's construction in that we use the effects/causes to faults/consequences relationships.

Constructing the BN involves making certain choices. For example, continuous nodes may be preferred to discrete ones, the choice here being a matter of compromise between complexity (and thus calculation time) and precision of the model. Whatever the decision made, the robustness of the learning methods of the BN needs to be tested and the physical representativeness evaluated by appropriate experts.

- The third stage consists in adapting the model to the dysfunctional operating modes based on the consolidated architecture obtained at the previous stage. Here, the detection capacity of the BN is tested. In other words, an analysis of its sensitivity to operational drifts and consequently its ability to detect faults. The dysfunctional operating mode database is created from DES by simulating preset multiple input faults (see Sec. 4.6 for details). The conditional probability matrices logically constitute the main output of this so-called deductive stage, since the inference rules now relate faults/consequences to effects/causes.

Once the model is consolidated, it will be operated to sort the possible causes of detected energy performance defects into hierarchical order [48].

2.3 Modeling of Energy Performance in Functional and Dysfunctional Modes.

The modeling the building's energy performance in its functional and dysfunctional modes (corresponding to the second and third stages mentioned previously) is itself divided into six steps (detailed in Sec. 4). The first step will consist in collecting the problem data. The inputs, i.e., the external and internal loads factors that influence the energy performance, are measured on-site. The outputs (heating needs), however, are simulated via TRNSYS (TRNSYS v17/type 56). A calibration sub-step had to be carried out in order to adjust the DES results to measured data from the test building. The second step will concern the choice and use of the accurate algorithm to learn from calibrated input and output data values, which have been first discretized in order to reduce calculation times. The third step tests the robustness of the BN; a process aided by the judgment of experts. The fourth step explores the effectiveness and influence of continuous nodes rather than discrete ones. The fifth step consists in developing a DBN from which we provide updated baselines from calibrated data. The sixth and final step is dedicated to the simulation of dysfunctional modes. We create new databases by means of DES with different faults situations from which the DBNs can be updated.

Figures 2(*a*)–2(*c*) give a conceptual representation of a BN modeling functional and dysfunctional modes. Occ_i (i = 1 to 3), Zone_j (j = 1 to 3), Syst_k (k = 1 to 3), Sens_n (n = 1 to 5) represent respectively the occupants, zones (or rooms) of the building, technical systems, and measurement sensors.

2.4 Control Charts for the Detection of Performance Faults and Drifts.

The principle behind the proposed modeling is that the fault detection can be viewed as a binary classification task: an observed state belongs to either the normal operation class ("under statistical control (SC)") or the faulty operation class ("dysfunctional" or "out-of-control"). A T^2 hotelling multivariate control chart [49,50] was used.

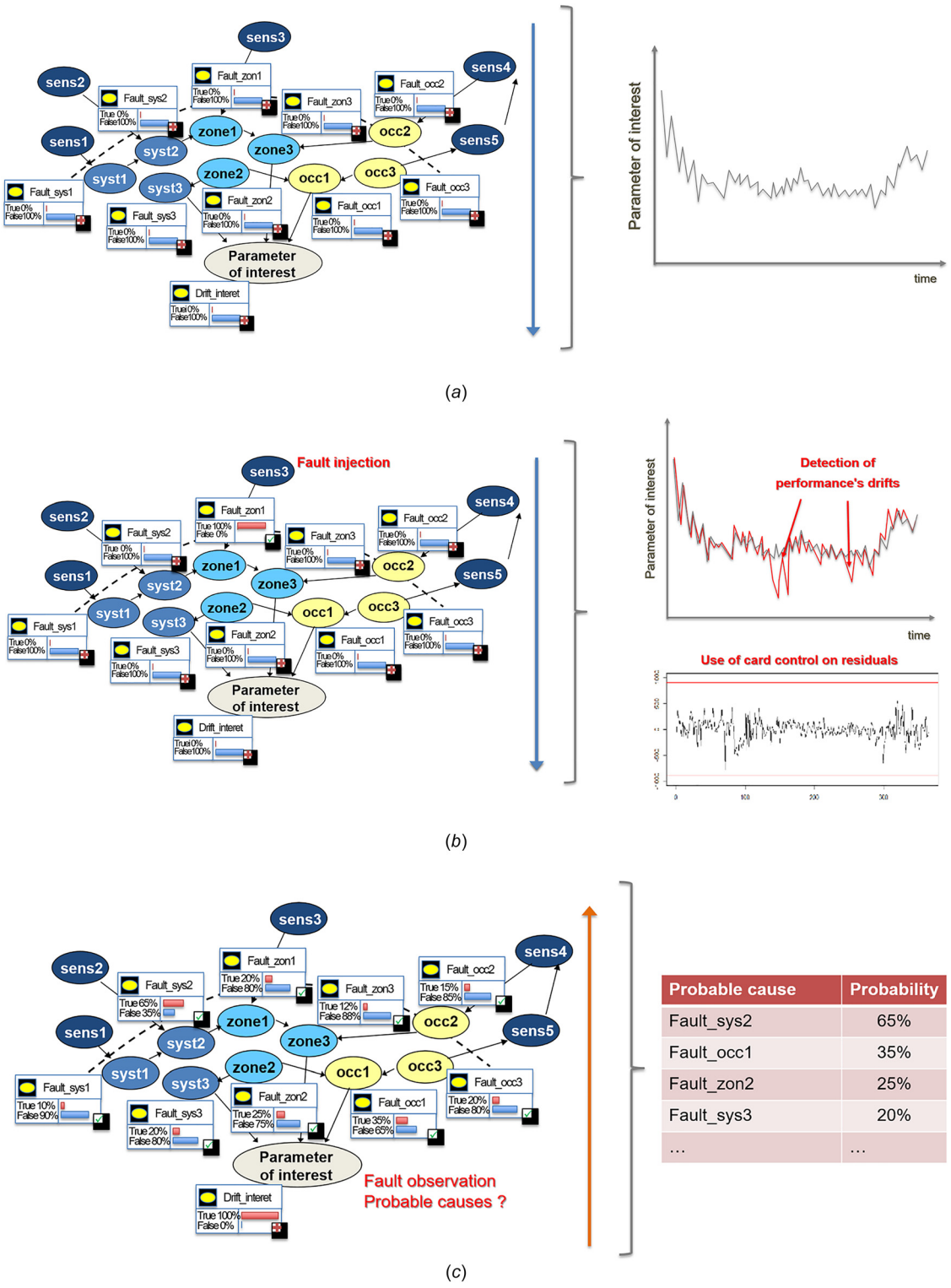

Probable cause	Probability
Fault_sys2	65%
Fault_occ1	35%
Fault_zon2	25%
Fault_sys3	20%
…	…

Fig. 2 Three stages of the proposed approach: (*a*) modeling principle for functional mode—inductive stage to establish "baseline" of behavior in functional (nonfaulty) mode, (*b*) modeling principle for dysfunctional mode—inductive stage to characterize effects of faults, and (*c*) modeling principle for dysfunctional mode—deductive stage to identify and hierarchize causes of performance drift

The detection of faults (dysfunctional or "out of control" states) in the Bayesian network modeling the system can therefore be considered by adding extra discrete nodes to the time-monitored variables—that means inserting control charts at key points for monitoring purposes. In this way, it is possible for example to detect abnormally high heating consumption compared with normal performance for the considered period, which might suggest a fault.

3 Case Study of a Building

3.1 Presentation of the Building. The building we choose for our case study belongs to CEREMA in Ponts-de-Cé, in France. A surface area of 105 m^2 was instrumented for the purpose of our study (see Fig. 3). This building was erected in the 1970s and is constituted of common aggregate blocks without insulation.

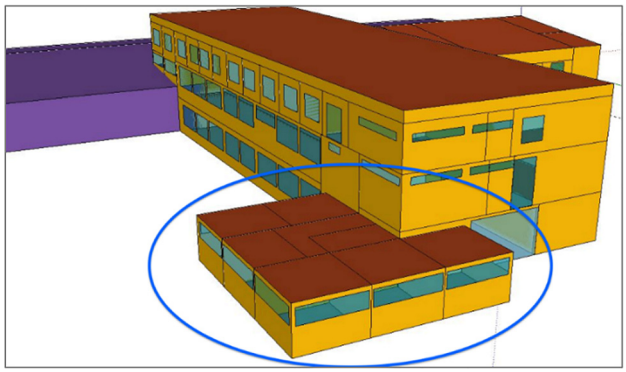

Fig. 3 Modeling using Sketchup 3D® of CEREMA building

Insulation was added to the suspended ceilings in the 1990s. The windows are double-glazed (4/6/4) with aluminum frames. The building uses mechanically controlled single flow ventilation. The heating is supplied by a standard high-temperature water loop system.

Some hundred sensors were installed to monitor temperature, caloric requirements, and occupancy level (see sensors installation in Fig. 4). Temperature gauges were placed in each room at a height of 1.50 m on interior partition walls, away from windows and doors. The caloric requirements were monitored using ultrasonic calorimeters placed at the entry of the heating water loop, meaning we may consider that the energy measured is used entirely for heating and that heating network losses are moreover recovered. In view of its complexity, it was decided to monitor the occupancy level using presence (passive infrared motion detection sensors) and windows' opening/opening sensors. The status of artificial lighting is also checked (with luxometers), and the loads due to plug-connected equipment are measured.

The TRNSYS tool was used to model the thermal performances of the building. The model was calibrated/trained with data collected by Caucheteux et al. [51] during a whole year from Jan. 1, 2013 to Dec. 31, 2013. Once trained, we have applied the model for a new heating period (151 days between the Oct. 1, 2015 and the Mar. 1, 2016) in order to assess the accuracy of our thermal model. We defined multizone models from the instrumented zones, and the Contam tool was coupled to TRNSYS for the airflow modeling (Contam is a multizone airflow and contaminant transport analysis program. It can help determine airflows such as infiltration, exfiltration, and room-to-room airflows in building systems driven by mechanical means, wind pressures acting on the exterior of the building, and buoyancy effects induced by the indoor and outdoor air temperature difference). The model included mechanical ventilation, air infiltration, and all opening of doors and windows. As regards air tightness, it was found that the majority of leaks came from windows. Therefore, for the purposes of the modeling, infiltrations were considered not just as proportional to the surface of walls but also linked to the quality of the openings. Finally, the occupants were modeled as "persons seated in thermal comfort at their workplace." The simulations were carried out to determine the caloric requirements in each zone (instrumented + modeled). In Figs. 5(*a*)–5(*c*), we present comparisons between simulated and real measurements for temperatures and required heat quantity (HQ). Specifically, Fig. 5(*a*) presents the variation of the required heat quantity as a function of the difference between indoor and outdoor temperatures for both simulated and real data. In Figs. 5(*b*) and 5(*c*), we give the details of the variation of the difference between indoor and outdoor temperatures and of the required daily heat quantity as functions of time (from the Oct. 1, 2015 to the Mar. 1, 2016). To assess the agreement between simulations and real results, we calculate the normalized mean bias error (NMBE) and the coefficient of variation of the root-mean-squared error (CV(RMSE)) which are two metrics recommended by both ASHRAE and IPMVP [52, 53]. Based on hourly measurements, we calculate a NMBE of −2.82% and a CV(RMSE) of 27.02%. ASHRAE guideline 14 and IPMVP, respectively, require that these values should not exceed 10% and 5% for NMBE, and 30

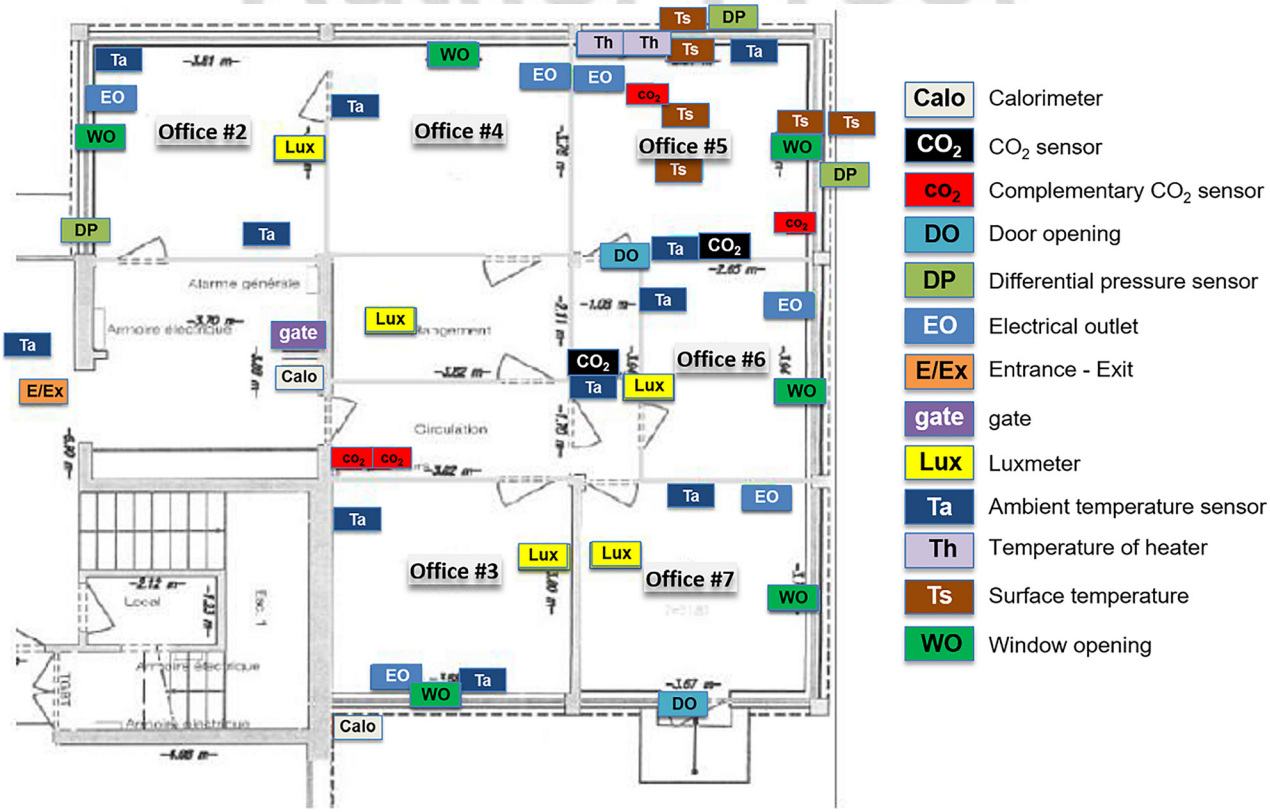

Fig. 4 Positioning of different sensors installed by CEREMA

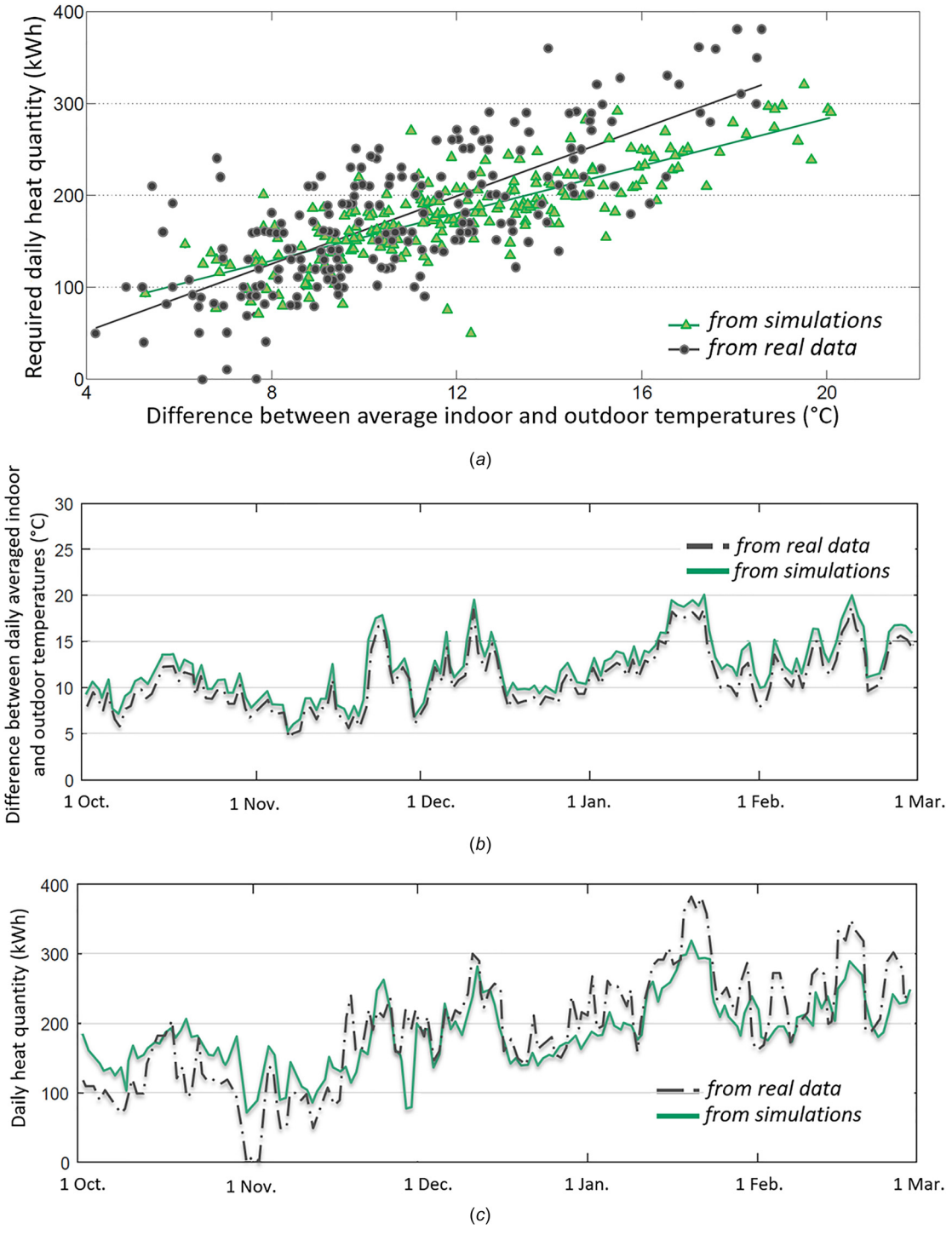

Fig. 5 Comparisons between the results obtained from DES model and actual data: (*a*) Variation of the required HQ (for the whole surface area of 105 m^2) as a function of the difference between indoor and OTs for both simulated and actual data, (*b*) variation of the difference between indoor and OTs as a function of time, and (*c*) variation of the required daily HQ (for the whole surface area of 105 m^2) as a function of time

and 20% for CV(RMSE). We must note that the CV(RMSE) calculated for our DES model is beyond the limit recommended by IPMVP. However, since we mainly use the model to detect differences between functional and dysfunctional situations and not to predict exact energy consumption, we finally consider that the DES is accurate in terms of our objective.

3.2 Characterization of External Loads–Meteorological Data. All variables of interest related to outdoor physical phenomena influencing the energy performances of the building were considered as external load factors. The first and best known of these phenomena is climatic conditions, which, with year-to-year variability, seasonality effects, and variations over time,

Table 1 Monitored variables

Calculated	Measured	
Occupancy level	Motion/presence sensors	Indoor/preset temperature
Interior sources	Entrance and exit of occupants	Surface temperature
AL due to windows' opening[a]	Opening/closing of windows and blinds	Supply air temperature
	Intensity of light	Pressure differential
	Concentration of CO_2	Heat energy consumption
	Electrical energy	

[a]This variable is deduced from the measurements but is not considered as an internal load. It is used along with the permeability, wind velocity, and relative pressure data to characterize the leakages.

determine the performance level required for a building and its equipment to ensure the comfort of its occupants.

In our study, dynamic meteorological data were collected via a weather station installed on-site. This was equipped with the temperature, relative humidity, global horizontal radiation, wind speed, and direction sensors.

The station location must be chosen in such a way that it comply with WMO recommendations [54], i.e., away from obstacles and in a grassy area. Wind speed measurements may sometimes by affected by certain external phenomena. The measurements taken were therefore broken down into two: light winds and strong winds. If the anemometer has a resolution of 1 m/s, only wind speeds above 1 m/s can be measured.

To complete the meteorological data, the renewal of air was monitored through the ventilation flow rates and the air permeability of the building. The flow-rate measurement of the single flow ventilation installed was achieved via by an air flow-rate measurement cone connected to a hot wire sensor or anemometer.

3.3 Characterization of Internal Loads. The behavior of building occupants can make it difficult to follow the conventional scenarios outlined by the regulations in place. People interact with their immediate environment searching for desired comfort level of which the most direct indicator is indoor temperature. In adjusting this temperature (or other systems), occupants influence the energy consumption.

Electrical equipment and appliances are supplementary sources of energy. These variables—indoor or preset temperature, number of occupants, internal sources—contribute to the building dynamics and have to be considered as internal loads. These interdependent variables are indirectly characterized via the installed sensors. Table 1 lists all variables that are directly measured or (indirectly) calculated.

Occupancy can become a significant internal load. By "occupancy" is meant the number of persons present in the building at a given time in conjunction with their behavior. The energy consumption of a building is directly linked to the occupancy rate as well as the behavior of the users. Workplace occupants can be a serious source of loss and this is a factor that affects the building dynamics: for instance, opening doors and windows necessitates an additional supply of heat energy in order to balance thermal losses. However, occupants can also be a source of energy by their activity. In our study, we have considered that every occupants are sitting persons in thermal comfort. Their metabolic rate is about 58 W/m^2/person (1 Met) [55] with a body surface for average adult of 1.7 m^2; therefore, the energy released by metabolism is taken at 100 W/person (direct energy source). Devices used by occupant (household appliances in a residential building and IT-related in a tertiary building) also supply energy to the building that can be quantified as an internal source (indirect energy source). This indirect energy source is dissociated from the occupancy and dealt with independently in the form of internal sources.

To estimate the occupancy level of a building, several estimators are used based on different measurement protocols that have been established [51–56]. They can be based on video recordings, measurement of CO_2 concentration, motion detection, noise analysis, or electricity consumption data [57,58]. The combination of several of these measurements provides more detailed information regarding the occupancy level and thus a reduction of the uncertainty of the estimation [59]. In our study, the occupancy level is characterized via measurements from motion detection sensors (passive infrared), CO_2 sensors, lux meters for artificial lighting, sensors for opening/closing of windows, and electricity consumption sensors for socket loads. As far as internal heat sources are concerned, it is quite a complex matter to measure the quantity of heat effectively released by occupants and electrical equipment. The most common practice consists in measuring electricity consumption and assuming that all the power consumed by electrical equipment is totally released within the building.

The indoor temperature is the ambient temperature of a room that is regulated via a preset temperature in order to achieve the desired thermal comfort. The indoor temperature can be measured in every room. In addition, surface temperature measurements can be taken, as well as measurements of the air temperature at the exit of the heating supply devices.

4 Construction of the Bayesian Network

The construction of the BN follows the six steps mentioned in the previous Sec. 2.3.

4.1 Step 1—Collection of Data and Prediction of Heat Quantities by Means of Dynamic Energy Simulations. The inputs and outputs of the model are shown in Table 2.

The indoor data were collected from a floor of the building with sensors installed according to the measurement plan shown in Fig. 4. The outdoor data were mainly obtained from our meteorological station and completed with data from a regional station. All the data were recorded from Jan. 1, 2013 to Dec. 31, 2013. The outputs are the predicted heat quantities in each room of the building; predictions were made through the DES model.

4.2 Step 2—Choice of the Learning Algorithm for the Construction of the Bayesian Networks. The construction of a BN consists mainly in finding the set of relationships (links) between variables (nodes) and the conditional probabilities tables between the thus linked variables. The goal here is to find the BN, with a controlled level of complexity, which best fits the training database and can give accurate predictions. We typically have to deal with a complex combinatorial problem, which first requires specific algorithms to detect conditional independences and then heuristic search in the solutions space. We have tested several current learning algorithms to find the one(s) that are the most appropriate for our problem. Table 3 shows all the different alternatives we have compared. Most of these inference algorithms dedicated to discrete nodes are available in the HUGIN software or toolboxes like BNT computed with MATLAB by Murphy [60].

From the same database, an algorithm alone can provide multiple nearly optimal solutions, and, another algorithm can give different candidate solutions. A way to compare the efficiency of the algorithms is to calculate the biased variances for each model

Table 2 Input and output variables of the model constructed by BN

Inputs (collected from Jan. 1, 2013 to Dec. 31, 2013)		Output (estimated from DES simulations)
Outdoor—meteorological data	Indoor—measured directly from sensors or calculated	Required HQ calculated individually for each room
Atmospheric pressure (AP)	AL	
Diffuse radiation (DR)	Internal heat gains (IG)	
OT	Indoor temperature (IT)	
RH	Presence or occupancy level (Pre)	
Solar Azimuth (SA)	Solar heat gains (SG)	
Solar height (SH)		
Total horizontal radiation (THR)		
Wind direction (WD)		
Wind speed (WS)		

Table 3 The different combined or hybrid learning algorithms

Search for conditional independence relationships	Hybrid algorithms
Grow-shrink	Restricted maximization
Incremental association	Max-min hill-climbing
	Max-min parents and children search
Heuristic search in solution space	
	Hiton parents and children search
Greedy search	Chow-Liu
Tabu search	Aracne search

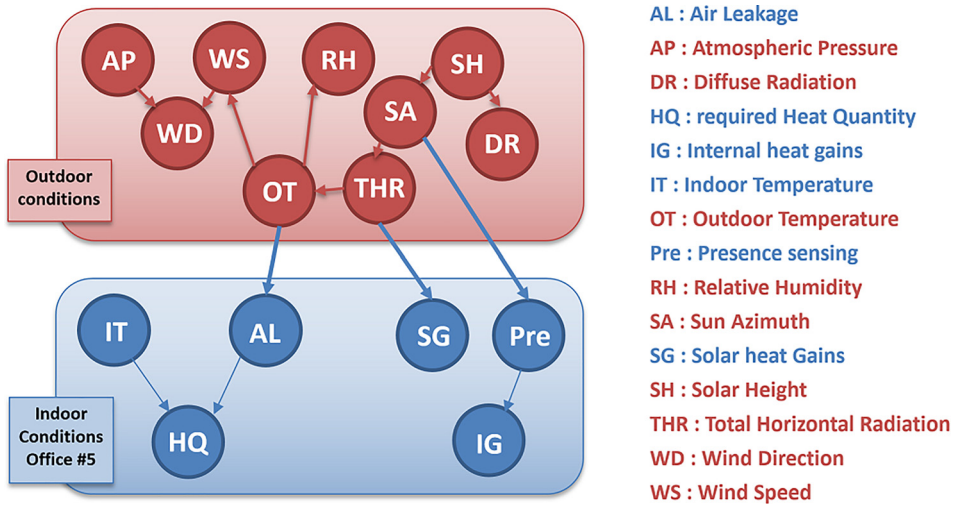

Fig. 6 Bayesian network for operational mode solely for Office #5 (with hourly measurements over a period of a year)

using an information criterion for the selection of the model (e.g., akaike information criterion (AIC)—or Bayesian information criterion (BIC)); the main concern here is to use the same score when comparing the BN architectures in order to choose the one which is the best in an objective way.

In order to test our method, we applied it to a single office (see Fig. 4—corner office #5) for which a large range of sensors and data were available.

Figure 6 shows the inputs (parent nodes) taken from meteorological data (upper part of the diagram) and those taken from measurements obtained from sensors inside the rooms (lower part). This figure reports one of the best candidate solution obtained, considering hourly measurements over the whole year, with nodes discretized via an algorithm based on AIC. The marginal probabilities and tables of conditional probabilities for the nodes were learned from a no-fault data file (since we are in operating mode).

It needs to be specified clearly that the purpose of our methodology is not to establish automatically the final BN architecture but just to give to the user a starting point reflecting visually the causal relationships between the various variables. Experts from a physical understanding of various phenomena must validate these conditionally dependences and independences. Their expertise is essential in the construction of the final BN architecture. Moreover, the experts may add or delete some arcs in the network if they consider that necessary.

As an example of causal relationships explanation, the network in Fig. 6 shows that the energy need (output of the child node) HQ, equivalent to the heating consumption, is directly dependent on indoor temperature IT but equally on the air leakage (AL) level AL of the envelope. However, the fact that the conditional distribution for each variable is defined according to its parents does not signify that no other variables influence it. Indeed, nodes IG and HQ are conditionally independent if and only if all the nodes

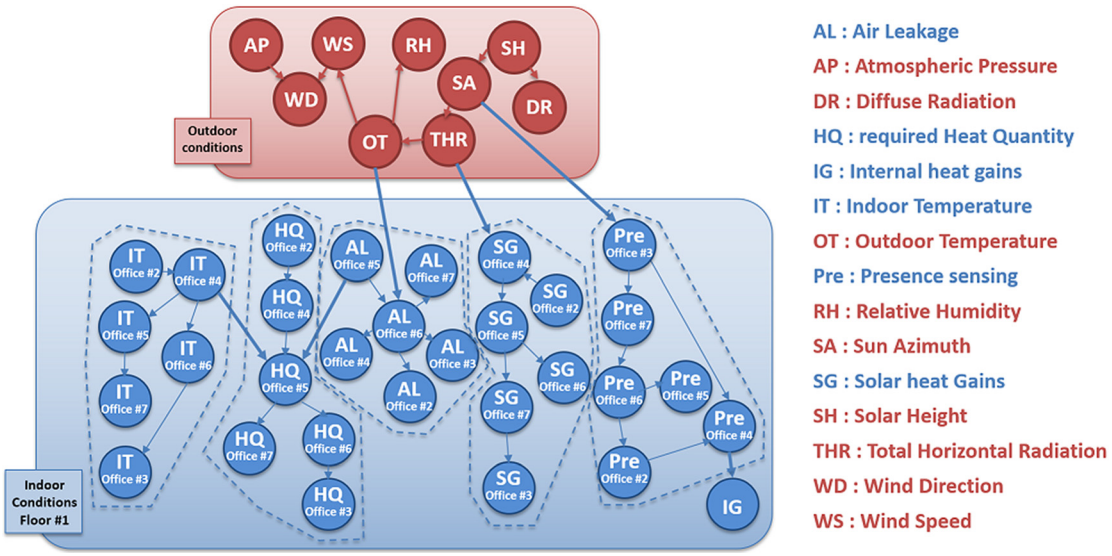

Fig. 7 Bayesian network for operational mode for whole floor (with hourly measurements over a period of a year)

belonging to the Markov blanket of IG (or HQ) are observed (i.e., one knows theirs values). Thus, in Fig. 6, HQ is conditionally independent of IG if the nodes IT and AL are observed. That means that knowing IG when IT and AL are observed does not change anything in the computation of the probabilities of the various modalities of the node HQ. Nevertheless, if AL is not observed, then IG influences the probabilities of the modalities of the node HQ because of the path: IG-Pre-SA-THR-OT-AL-HQ. In addition, the OT node influences the HQ if AL is not observed. From a physical point of view, if the AL is inexistent (perfect air-sealing quality) the OT should not influence the HQ (i.e., HQ is influenced by OT only if AL exists).

The same task of modeling the operational mode by BN was carried out for a whole floor by "forcing," during the network architectural stage, the grouping together of variables of the same-type (for example, heating consumption HQ for offices nos. 2–7 combined). The relationships between nodes of the same type are shown with thin-lined arrows. The relationships between nodes of different types (for example, OT and air leakage in the office #6 AL_Office#6) are shown with thick-lined arrows. Of course, many number of different BN models for operational mode are possible, limited only by the extent to which the physical coherence of the relationships established between the network variables can be justified. In Fig. 7, we show the BN adopted based upon a minimized BIC index, from which we can discuss some examples of causal relationships. Physically, there is a link between outdoor (OT, RH) and indoor (indoor temperature (IT)) conditions. The network shown in Fig. 7 proposes a link between RH and the AL. It is not what was first expected, but the link is consistent. Indeed, considering that AL can be regarded as a heat loss by air leakage, there is an obvious link with the outdoor conditions. Some links are less intuitive. For example, the link between Solar Azimuth (SA) and people presence (Pre) was unexpected. Nevertheless, if we consider the correlation between SA and the hour of the day, it is now obvious to see a relationship between the hour of the day and the presence of people. Of course, all relationships can be discussed but a coherent explanation can be provided for most of them and the BN can be consider as acceptable.

4.3 Step 3—Study of the Bayesian Networks Robustness Against Database Reduction. The ability of a BN to detect and diagnose faults is conditional upon its robustness against parameters related to the data exploitation or extraction. We need to check if the general architecture of the BN and its capacity to model the data is deeply modified when we consider only a part of the database or when we take the average of the hourly measurements on a daily base. The main objective is to see eventually if we can construct a BN with equivalent quality but with fewer data to process.

First, keeping to the same hourly measurements, we have reduced the database to data for which heating consumption was different from zero for all offices. We thus excluded data for which an energy need had not been calculated for at least one of the six offices. The new BN obtained in this case is presented in Fig. 8. Comparison to the equivalent BN with the complete database shows only minor changes in the relationships between variables of the same type and in the relationships between types. Only one significant relationship appears (see black thick arrow), between the indoor temperature in office #6, IT_office#6, and the energy need in this office HQ_office#6. Therefore, this first modification of the quantity of data taken into account and the very slight change of the BN seems to demonstrate the robustness of our method and that we can reduce the database to the periods recording energy needs.

The second test consists in modifying the frequency of data acquisition. Here, we examined the sensitivity of the BN to a change from hourly to daily measurements; the inputs are the averages of the values recorded over a day for all characteristics measured (including, e.g., wind direction, in degrees). In Fig. 9, we show the new BN modeling the relationships between variables for the whole floor #1 reducing data to daily measurements over a period of a year. The results are interesting: although a large majority of the internal relationships between nodes remains after change of frequency of measurement, one can see a higher number of new links between characteristics of different types (see black thick arrows).

The two BN's robustness tests we have conducted allow us to conclude that we can use a reduced part of averaged data with small disturbances of the BN architecture and of its efficiency. The calculation time decreases which will be useful when we will adopt continuous nodes rather than discrete ones in step 4 (Sec. 4.4) and when we will need to develop DBNs in step 5 (Sec. 4.5).

4.4 Step 4—Choice of Type of Nodes. In the following steps, having confirmed the effectiveness of the construction method of the BNs for the purposes our study, we choose to not discretize the nodes in order to avoid any loss of information; all the nodes will be modeled from continuous statistical distributions. We maintained the assumption that they follow a Gaussian distribution law and that they are not interlinked via linear

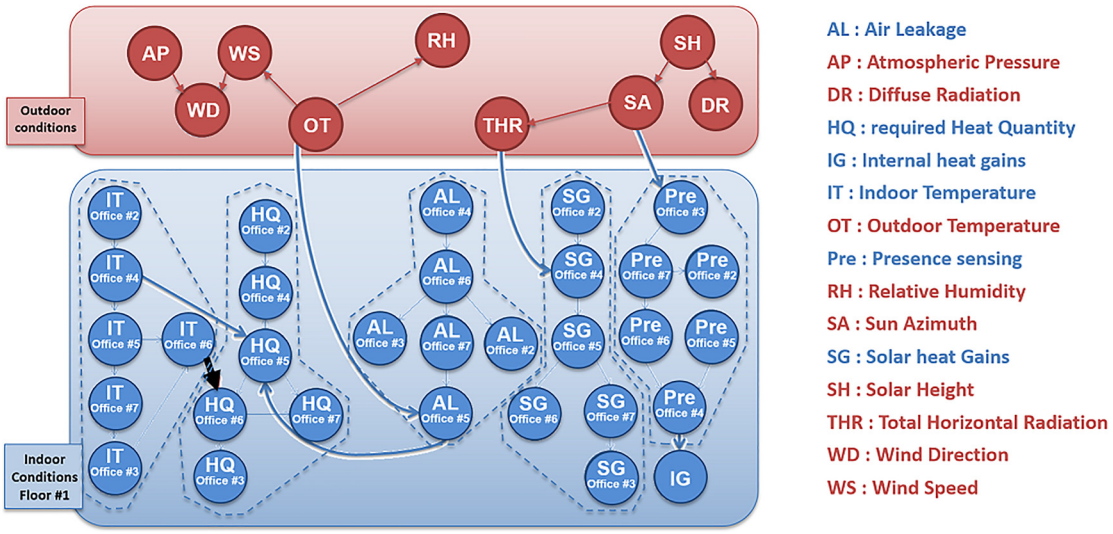

Fig. 8 Bayesian network for operational mode for whole floor (using hourly measurements during period of heating only)

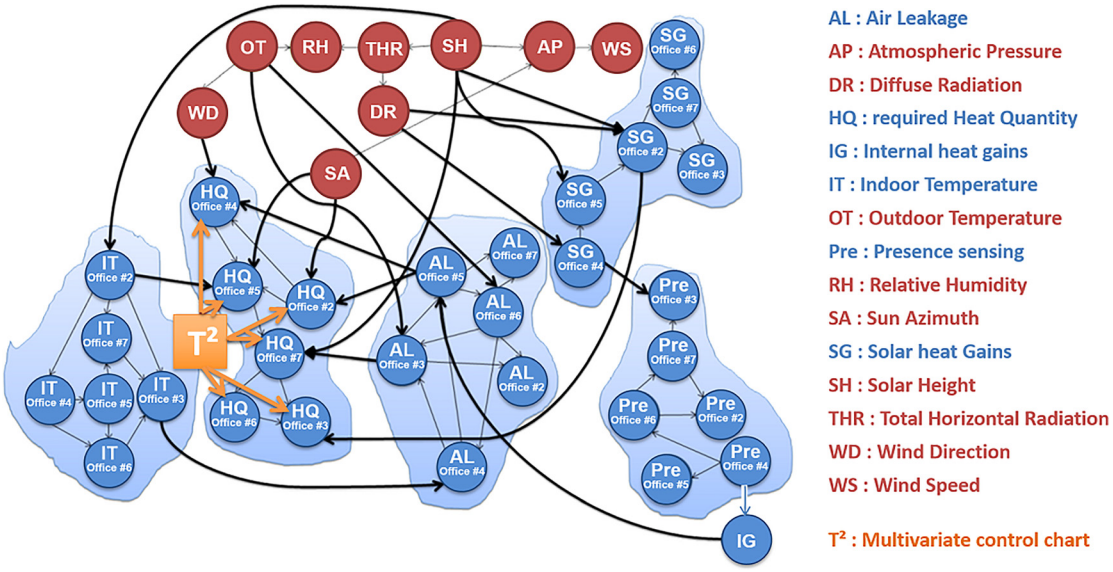

Fig. 9 Bayesian network for whole floor (using daily measurements over a period of a year). Implementation of a T^2 Hotelling multivariate control chart to detect drifts of the energy needs is also illustrated.

dependency relationships. It should be noted that these assumptions can change depending on whether one deals with a discrete or a specific inference node (nonlinear non-Gaussian).

Once the network structure and its parameters are defined, it is essential to use propagation algorithms that are appropriate to the chosen structure in order to calculate marginal distributions as well as probability distributions for each variable. Several inference algorithms have been suggested in the literature for Gaussian conditional networks. We used two algorithms based on the junction tree [61,62]. We implemented them with the *R* scientific computing environment. These algorithms allow accurate inference in Gaussian conditional networks.

We also wanted to guarantee better AIC or BIC scores (information criterion) for the choice of BN models. It is therefore necessary to reduce the impact of local optima during optimization of the architectures and parameters of the BNs. We thus adopted the bootstrap resampling method already used in Sachs et al. [63]. In practical terms, this consists in repeating the learning of the structure several times, which allowed us to explore a large number of networks, to average the networks obtained (see Ref. [64]) and to finally conserve only the relationships (links) that were present in at least 85% of the networks. Figure 10 illustrates the final BN obtained with continuous nodes. Some changes are observed between this BN and the one obtained with discrete nodes, but the general architecture remains. The BIC score for this BN with continuous nodes is nearly the same that for discrete nodes (−49,727 versus −50,523, i.e., a sensible loss of 1.6%). We will use continuous nodes for the upcoming simulations with the aim to obtain results that are more accurate.

4.5 Step 5—Creation of Bayesian Network in Dynamic Mode. The DBNs are a special class of BNs; it includes the effect of time by considering that the value of a variable at a given time can influence its own value at the next time [65]. If we consider a set of n variables $\boldsymbol{D}(t) = \{D_1(t); D_2(t); \ldots; D_n(t)\}$ varying with time, a DBN adds the joint probability distribution of these variables for a bounded interval $[0; T]$. Generally, this distribution can

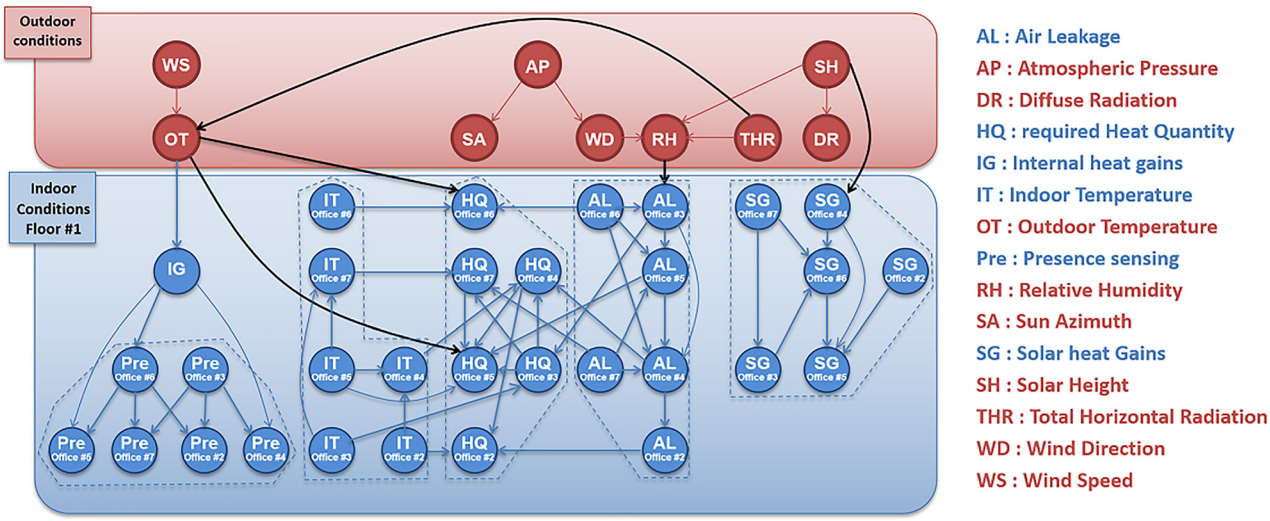

Fig. 10 The Bayesian network for whole floor (using daily measurements over a period of a year) with continuous nodes

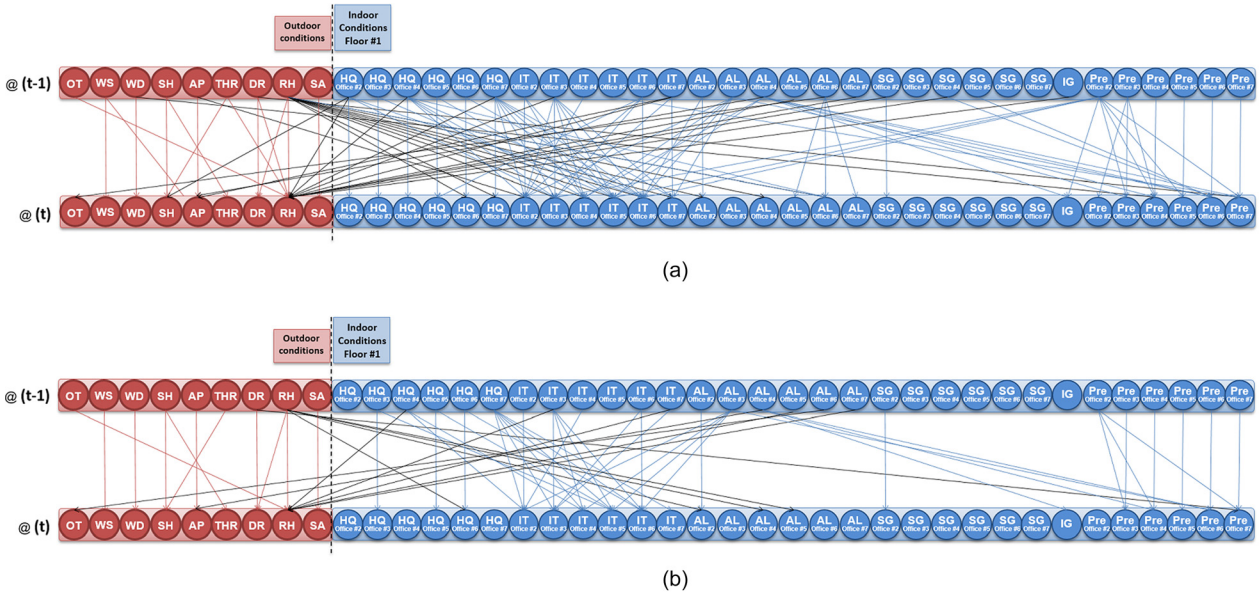

Fig. 11 Illustrations of a dynamic Bayesian network with two different levels of significance: (*a*) Relationships between variables at ($t-1$) and (t) for a level of significance p-value < 0.01 and (*b*) relationships between variables at ($t-1$) and (t) for a level of significance p-value < 0.001

be expressed as a static BN with $T \times n$ variables where T is the number of time intervals considered. If the process we consider to model is stationary, the assumptions of independence and the associated conditional probabilities are identical for all time intervals $\Delta t=(t) - (t-1)$. In this case, the DBN can be represented by a BN whose structure is duplicated for each time-step. A node therefore represents a random variable whose value indicates its state at time t.

The DBN are widely studied by researchers. In the domain of energy optimization, DBN are used as a prognostic approach for modeling aggregated load of HVAC systems [66,67], for detecting occupant's interactions with windows [68] or for evaluating the reliability of grid-connected photovoltaic systems [69]. In our case, the prognostic capacity of DBNs is an important improvement in the anticipated detection of operational faults and drifts. Given that the number of dimensions rises as a result of the introduction of the time factor, the problem of optimization related to this choice of BN model may be dealt with via the "least absolute shrinkage and selection operator" or LASSO algorithm explained in [70]. Interested readers may use the "lars" package for *R* software in order to make computations.

Figures 11(*a*) and 11(*b*) present the (repeatable) relationships between the variables of the BN at times ($t-1$) and t for two levels of significance p. This p-value corresponds to the probability that the hypothesis of an existing relationship between two variables at two consecutive times is null. In the following simulations, we have only considered the relationships with a p-value of 0.001, which in addition contributes to reduce the complexity of the DBN and the simulations time.

Figure 12 illustrates how a DBN can be used to predict energy needs or the heat quantity in office #6 (HQ_office#6) using relationships of dependence between time t and $t-1$. The curve with the continuous orange line shows the results of simulation by DBN for the predicted/probable values of heat quantity HQ_office#6 with time (for a time sequence t), considering the values for all other variables at instants $t-1$ and t. The inputs are daily measurements, and the curve shows energy needs over a year. The dashed blue line on the same figure gives real heat quantity

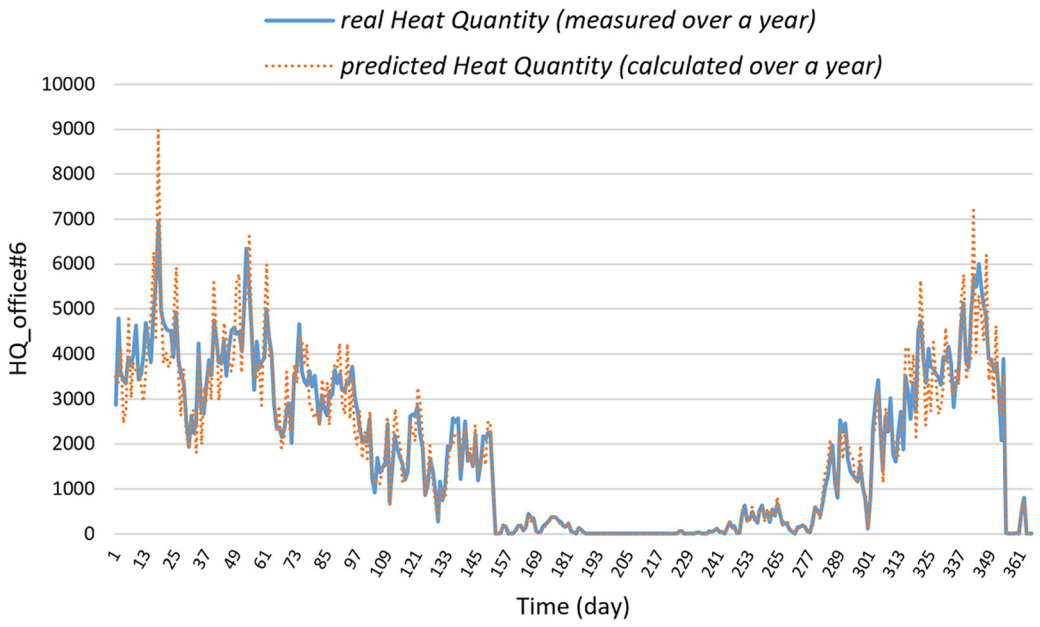

Fig. 12 Energy needs (or HQ) of office #6 (HQ_Office#6)

HQ_office#6 measured over the year. The fit between the two curves is very good as long as the target variable HQ_office#6 is calculated with all the available information (including the heat quantities of other offices, HQ_office#*j*). In terms of metrics of comparison between the actual and simulated heat quantities, we found values of NMBE and CV(RMSE) respectively at −3.8% and 18.7% which are still below the threshold values recommended by ASHRAE Guideline [52] and IPMVP [53]. For complete information, the Frechet distance between actual and predicted values is estimated at 2703. Regarding more precisely the fit of the two curves, it is worth pointing out that the simulations give a lot of noise for the "warm" period, which, however, is of no consequence in the context of assessment of the overall performances guarantee. Therefore, we can estimate that the use of DBNs for this inductive stage to setup a "baseline" (see Fig. 2(*b*)), from which to detect faults and drifts, is relevant.

4.6 Step 6: Experiment Design Used for Simulating the Effects of Fault Situations. Once the baseline corresponding to the normal operating conditions has been obtained, the following step is used to simulate the effects of small faults on the dynamic performances of the building. Then, we create a new database by means of DES with different faults situations from which the DBNs can be updated. It is important to underline that, for this step, we consider that the architecture of the previous DBNs obtained in step 5 is stable; the updating will only concern the conditional probability tables. This makes the assumption that the faults effects, of which amplitudes still remain controlled at the (early) time of detection, had a priori been modeled by the previous DBNs, considering the whole ranges of the variables values of the learning database that encompass the faults amplitudes.

From the 14 input variables (the 15th variable is the output heat quantity) constituting the basis of the DBN, only a part of them are directly requested as factors for the dynamic energy simulations. All other variables depend on additional factors. Table 4 summarizes the 13 factors for which we have studied the effects of possible deviations from normal conditions. The fourth first factors are variables from the DBN, the nine others are factors on which depend the remaining ten variables of the DBN. In our DESs, the deviation could be either positive or negative depending on whether the fault corresponds to a deficit or an excess (i.e., to a high or low performance threshold). In order to update the DBN, 104 multiple-fault situations have been simulated by DES. These situations are summed up in Table 10 in Appendix; all the assumptions and data shown in this table are reported in Ref. [56].

5 Simulation and Results

5.1 Results for Certain Simulated Faults. Once the 104 fault situations are simulated by DES, we have studied various fault situations in order to test the FDD capabilities of the updated DBNs. In order to avoid overloading the display of the results, only the consumption in office 2, HQ_office#2, is analyzed here.

Because of the density of the measurements, it is difficult to distinguish the differences between the fault situations and the baseline, referenced as "E0." Therefore, we limit the comparison of the results to the period from 900 to 1800 h.

Figures 13 and 14 illustrate two examples of simulation of energy consumption deviations in office 2 following the appearance of faults. These figures show the deviations of the energy consumption between the baseline E0 and two fault cases. The first one (referenced as "case_1") consists in an increase in the preset temperature of +1 K (see Fig. 13) and the second one (references as "case_2") is a drift of the glazing transmission coefficient of $-0.5\ \mathrm{W/m^2\ K}$ (see Fig. 14). In case_1, the injected fault on IT leads to an average relative discrepancy of performance equal to +7.64% (with a standard deviation of +6.34%. In case_2 (injected fault on *Uwi*), we observe respectively values of +1.86% and +2.02% for the average discrepancy and the standard deviation. One will note that the first fault has a higher effect than the second one.

Figure 15 illustrates the probability of a process being under SC $P(\mathrm{SC}/x)$ over time in the case of an increase in preset temperature. The faults are injected independently at time $t_1 = 1000$ h and the simulations are stopped at $t_2 = 1800$ h. Here, it is worth pointing out, since only one variable—HQ_office#2—is analyzed, that the T^2 Hotelling chart is reduced to one chart, "*Xbar and S*." Given that case_1 is a simulated fault situation, a very rapid and very clear drop of probability $P(\mathrm{SC}|x)$ can be seen after the injection of faults at $t_1 = 1000$ h. It is therefore very quick and easy to detect fault situations. But, what is really of interest, and this is the advantage of using BNs, is the ability to carry out a diagnosis, i.e., to determine the most probable initial cause of the fault.

For the same detection threshold (here, for example, $P(\mathrm{SC}/x) = 0.6$) and measurements obtained over a control period of 6 h (c.f. Sec. 5.4. *Influence of control period* below for a

Table 4 Simulation variables for fault situations

Factors	Code	Low-performance threshold	High-performance threshold
AL (coefficient)[a]	AL	2	0.5
Indoor temperature *or preset temperature* (K)[b]	IT	+1	−1
Internal heat gains (coefficient)[c]	IG	1	2
Level of occupancy (coefficient)[d]	Pre	1	2
Albedo ( )[e]	Alb	0.1	0.4
Glazing solar factor (coefficient)[f]	GF	−0.2	+0.2
Ground temperature (K)	GT	−3	+3
Low ceiling (coefficient)[g]	LC	0.5	1.2
Thermal bridges (coefficient)[h]	TB	1.2	0.8
U_{roof} or High ceiling (coefficient)[g]	UR	0.5	1.2
U_{wall} (coefficient)[i]	Uwa	0.78	1.62
U_{window} (W/m^2 K)[j]	Uwi	3.2	4.2
Ventilation (kg/h)[k]	Ve	200	100

[a]AL: the air permeability coefficient of the nominal situation was taken to be equal to 1.7 m^3/h.m^2. The dispersion typically observed on buildings erected between 1948 and 2000 was retained, which corresponds to a disturbance of the default value by a multiplicative coefficient of between 0.5 and 2. For instance, the low performance level corresponds here to an air permeability of 3.4 m^3/h.m^2.
[b]Indoor or preset temperature: the preset temperature uncertainty equates to the measurement uncertainty of the indoor temperature, which covers sensor uncertainty and spatial sampling uncertainty, i.e., ±1 °C.
[c]Internal heat gains: it corresponds to heat power from electrical devices use. Its uncertainty can be large if not precisely measured.
[d]Level of occupancy: The occupancy measurement procedure (via motion detection) was affected by a bias consistently tending toward underestimation, due to the possible absence of motion during occupancy as well as the possible presence of multiple individuals in a single office. A disturbance of hourly occupancy of a factor of between 1 and 2 was therefore applied.
[e]Albedo: it is a coefficient (between 0 and 1) that corresponds to the reflective power of external surfaces around the building. The dispersion comes from the uncertainty of the value (that is usual not measured) and the diversity of surfaces around the building.
[f]Characteristics of the bays: to represent the uncertainty of the thermal and radiation characteristics of the bays, the modeling variables of the glazing system (woodwork included) are disturbed by the method described in the appendix. The transmission (total and visible) multiplication coefficient for the glazing was considered to be between 0.8 and 1.2: this corresponds to a solar disturbance factor of ±20% around the basic value of 0.81.
[g]Low and high ceilings: the corrective coefficients applied correspond to an insulation thickness of between 10 cm (0.5 × 20 cm) and 24 cm (1.2 × 20 cm); 20 cm being the nominal thickness.
[h]Thermal bridges: the chosen dispersion deals with uncertainty of the materials and its implementation in the building.
[i]Exterior walls: the maximum dispersion of the thermal resistance of the air knives from the ThU rules was retained, i.e., between 0.11 and 0.23 m^2 K/W (nominal value $U_{wall} = 7$ W/m^2 K).
[j]Windows: The amplitude of the disturbances applied to the conductivity of the filling gas and the thermal transmission coefficient of the woodwork resulted in a variation of transmission coefficient for the glazing system ($U_{windows}$) of between 3.2 and 4.2 W/m^2 K.
[k]Nominal ventilation flow rate: ventilation flow rate was measured by the cone method. The measured value was 150 m^3/h. The experimental measurement conditions led us to increase this uncertainty and retain a dispersion of between 100 and 200 m^3/h.

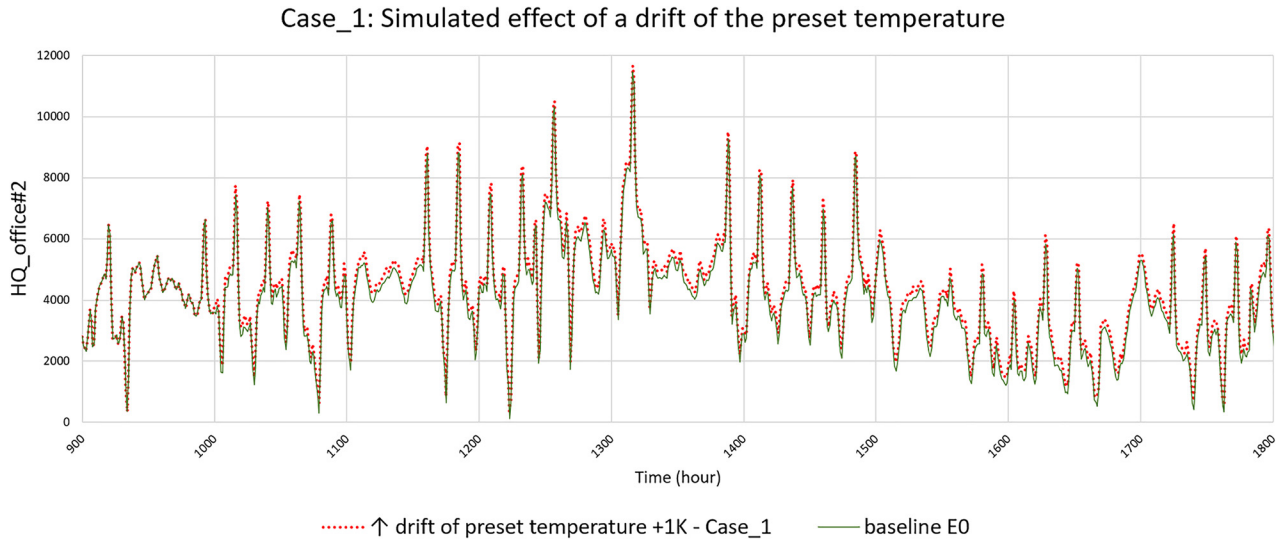

Fig. 13 Simulation of consumption deviations for an increase in preset temperature (case_1)

definition), the fault is more rapidly identified in fault case_1 (21 h) than in fault case_2 (463 h ≈ 19 days). This fact is intrinsically linked to the amplitude of the faults effects. In case−1 we have a simulated average deviation of 249.7 and standard deviation of 53.5, and in case_2, a mean and standard deviation of 56.1 and 34.1, respectively.

Detection time is an important performance indicator. It depends on various factors; of course, on the amplitude of the fault effect on heat or energy needs HQ, but also on the value of the detection threshold $P(SCl_x)$, and on the width of the control period. Detection time is also stochastic in that it depends on the fault injection time. Figure 16 presents the distribution laws of

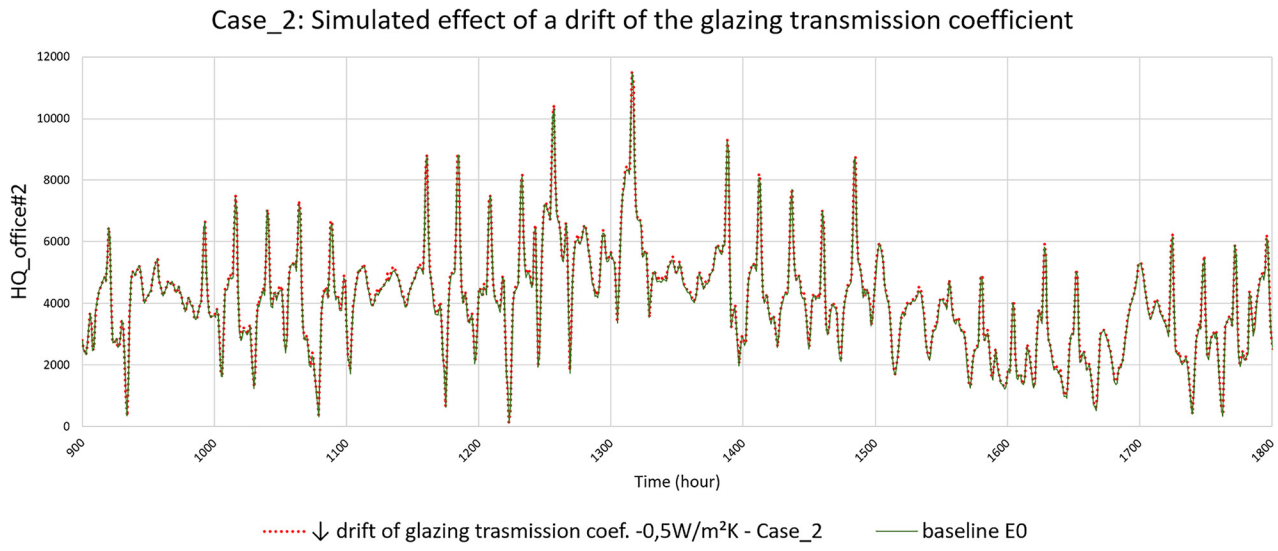

Fig. 14 Simulation of consumption deviations for a deterioration in glazing transmission coefficient (case_2)

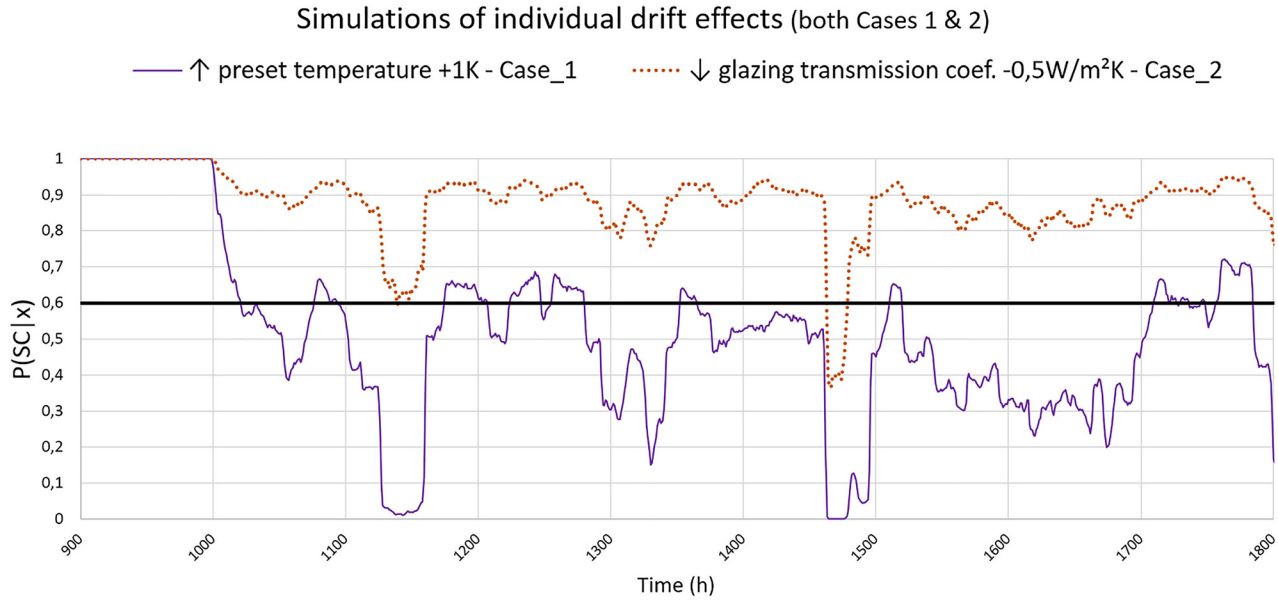

Fig. 15 Probability of being under SC after an increase in the preset temperature (case_1) or a decrease in the glazing transmission coefficient (case_2)

detection times for a preset temperature and a glazing transmission coefficient drifts for statistically injected fault times taken, for example, between 1000 and 2000 h and for the same detection threshold of 0.6 and with a control period of 6 h. For a very significant effect on energy needs (case_1 of a positive drift of the preset temperature), detection times are short and their distribution follows an exponential law. For a less significant effect (case_2 of negative drift of glazing transmission coefficient), detection times are longer and their distribution follows a lognormal law.

If the detection time in case_1 is shorter, it is more difficult to identify the possible causes (and hierarchize them). In fact, the more quickly the fault is identified, the more limited the quantity of available information is, and the more random the characterization of the fault will be. Table 5 shows a sorted list, obtained via a BN coupled with control chart, of probable causes of faults. The results have been standardized, and the sum of all the percentages for all 13 variables should equal 100%.

A lack of discrimination of possible causes is plainly evident in case_1: while the first six causes listed do represent 82.8% of the possibilities, the cause at the top of the list is only 2.3 times more likely than the sixth one. Moreover, the IT variable which is the actual cause of the fault [IT for indoor temperature (or preset)—see Table 4] is not identified as being the most possible cause. In this specific case_1, we think that the weakness in characterizing the fault is due to the fact that the deviations generated by the simulation in the first times after t_1 were greater than the average of 249.7 (which is what was measured between the time the fault was generated at 1000 h and the end of the simulation at 3400 h).

In case_2, the drift has been characterized correctly. The detection threshold is still 0.6, and the drift is identified after 463 h of operation in degraded mode: having recourse to more comprehensive information, the BN offers clear identification of the cause of drift, which is *Uwi* (U_{window} coefficient). *Uwa* is identified as the second most possible cause, however, with 2.8 times less likelihood of being the cause. It seems logical to assume that *Uwa* appears as a probable cause because the effect of injecting the fault into *Uwa* only (in a simulation not shown here) gave a simulated mean deviation of 61.8 and standard deviation of 39.8, in

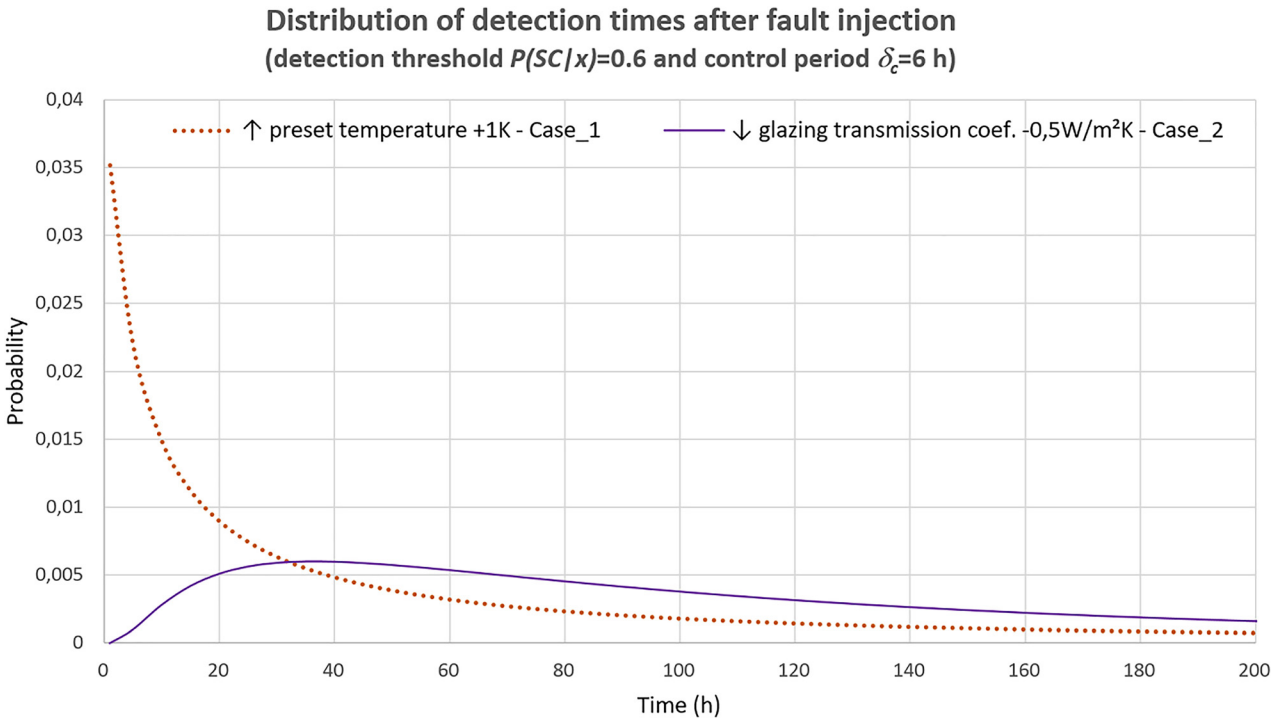

Fig. 16 Statistical distributions of detection times after an increase in the preset temperature (case_1) or a decrease in the glazing transmission coefficient (case_2)

Table 5 Ranking in descending order of possible causes of faults or drifts [detection threshold = 0.6 – control period = 6 h]

Fault/drift	Detection time (h)	Probable cause #1	Probable cause #2	Probable cause #3	Probable cause #4	Probable cause #5	Probable cause #6
IT (K) (or preset)	21	IG → 20.2%	IT → 17.0	Uwa → 13.3	Uwi → 13.0	TB → 10.7	AL → 8.6
U_w (W/m^2.K)	463	Uwi → 48.2%	Uwa → 17.1	TB → 6.5	AL → 4.0	UR → 2.9	Alb → 2.2

where AL is the air leakage, IT is the indoor or preset temperature, IG is the internal heat gains, Pre is the level of occupancy, Alb is the albedo, GF is the glazing solar factor, GT is the ground temperature, LC is the low ceiling, TB is the thermal bridges, UR is U_{roof} or high ceiling, Uwa is U_{wall}, Uwi is U_{window}, and Ve is the ventilation.

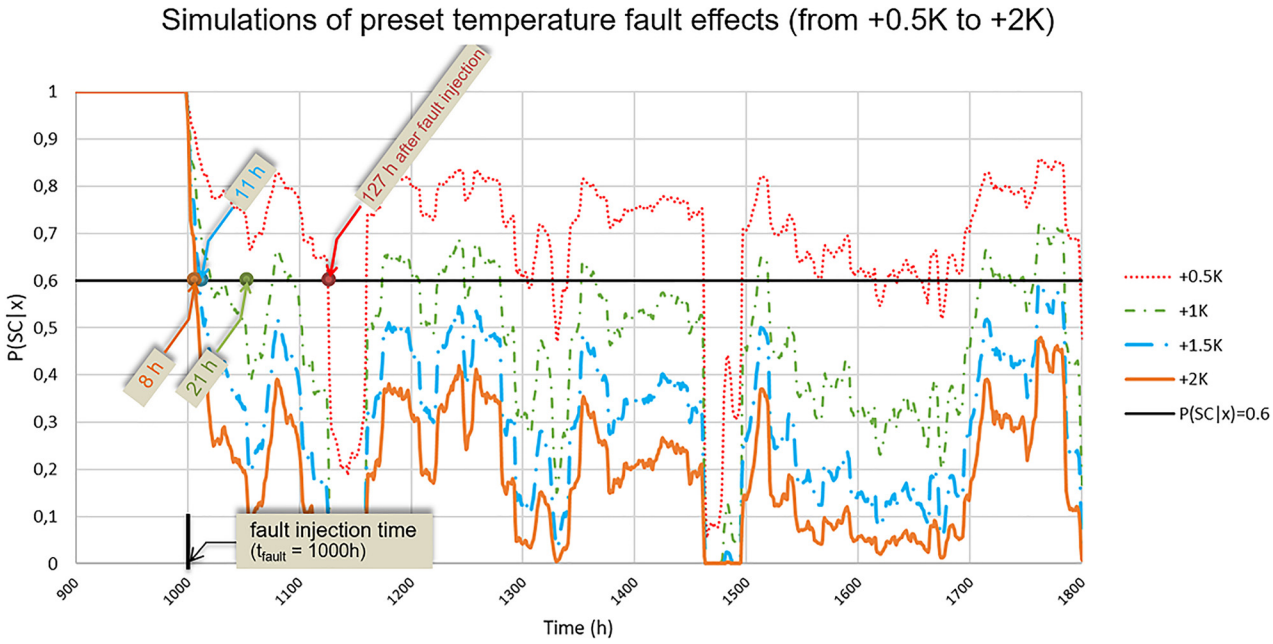

Fig. 17 Influence of the preset temperature drift amplitude on the probability of process being under SC

Table 6 Influence of drift amplitude (case_1 of preset temperature) on ranking of probable causes of faults [detection threshold = 0.6; control period = 6 h]

Drift amplitude	Detection time (h)	Probable cause #1	Probable cause #2	Probable cause #3	Probable cause #4	Probable cause #5	Probable cause #6
Drift of +0.5 K	127	IG → 19.1%	IT → 14.7%	Uwa → 12.2%	Uwi → 12.0%	TB → 11.2%	AL → 10.9%
Drift of +1 K	21	IG → 20.2%	IT → 17.0%	Uwa → 13.3%	Uwi → 13.0%	TB → 10.7%	AL → 8.6%
Drift of +1.5 K	11	IT → 38.1%	IG → 15.1%	Uwi → 11.2%	Uwa → 11.0%	TB → 6.2%	AL → 3.9%
Drift of +2 K	8	IT → 78.2%	IG → 5.1%	Uwi → 4.2%	Uwa → 3.0%	TB → 1.1%	AL → 0.8%

where AL is the air leakage, IT is the indoor or preset temperature, IG is the internal heat gains, Pre is the level of occupancy, Alb is the albedo, GF is the glazing solar factor, GT is the ground temperature, LC is the low ceiling, TB is the thermal bridges, UR is U_{roof} or high ceiling, Uwa is U_{wall}, Uwi is U_{window}, and Ve is the ventilation.

Table 7 Influence of threshold value on ranking of probable causes of faults [control period of 6 h]

Threshold value	Detection time (h)	Probable cause #1	Probable cause #2	Probable cause #3	Probable cause #4	Probable cause #5	Probable cause #6
Threshold of 0.6	21	IG → 20.2%	IT → 17.0%	Uwa → 13.3%	Uwi → 13.0%	TB → 10.7%	AL → 8.6%
Threshold of 0.5	53	IT → 40.1%	IG → 14.0%	Uwa → 12.2%	Uwi → 11.8%	TB → 8.8%	AL → 5.6%
Threshold of 0.4	114	IT → 78.2%	IG → 5.1%	Uwi → 4.2%	Uwa → 3.0%	TB → 1.1%	AL → 0.8%

where AL is the air leakage, IT is the indoor or preset temperature, IG is the internal heat gains, Pre is the level of occupancy, Alb is the albedo, GF is the glazing solar factor, GT is the ground temperature, LC is the low ceiling, TB is the thermal bridges, UR is U_{roof} or high ceiling, Uwa is U_{wall}, Uwi is U_{window}, and Ve is the ventilation.

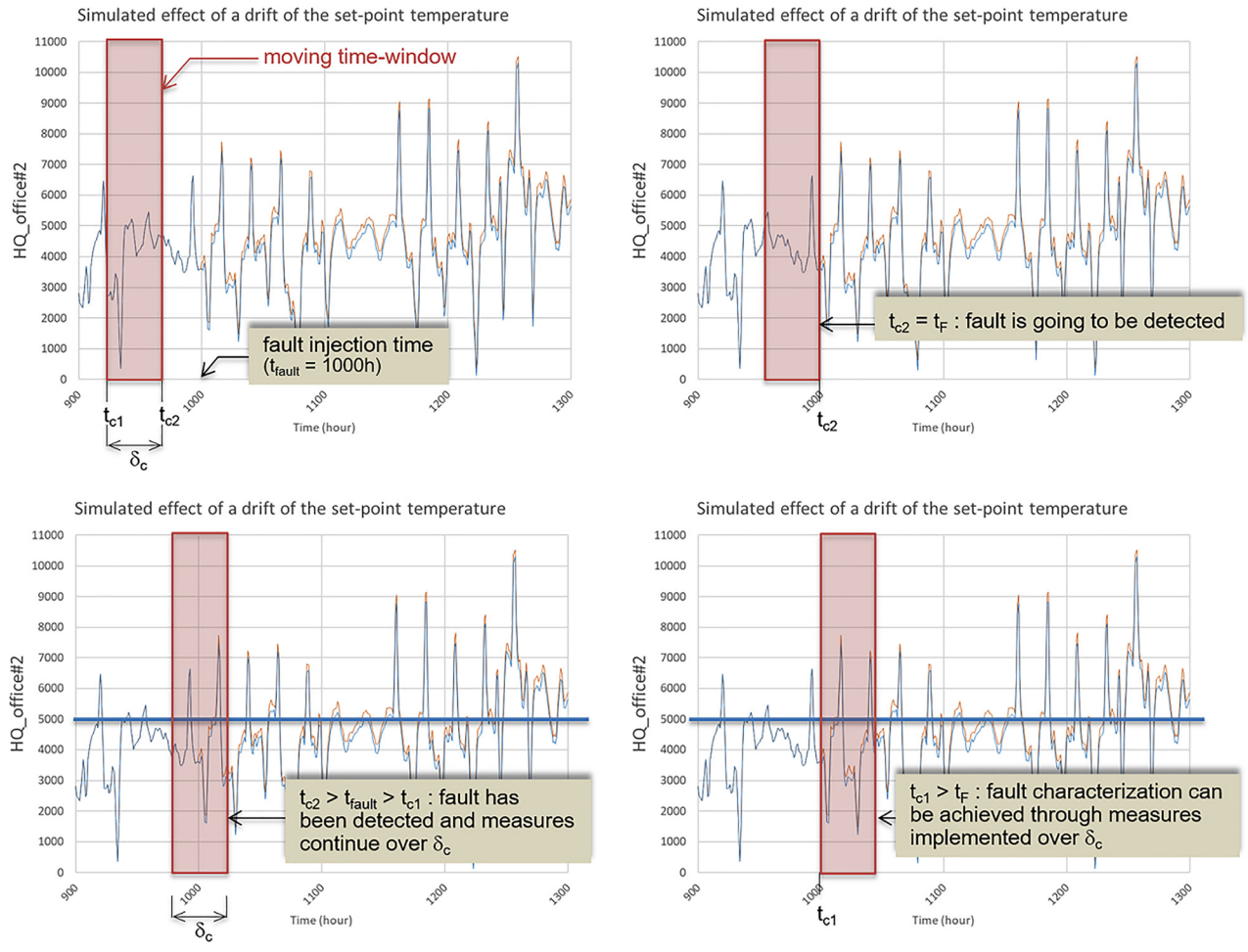

Fig. 18 Principle of the fault characterization moving time-window

other words, values that are very close to the simulated ones for *Uwi* only: 56.1 and 34.1.

5.2 Influence of Drift Amplitude. The influence of the drift amplitude has been suggested in the previous paragraphs. Here, we study this influence by considering the effect of different values of positive preset temperature drifts. To some extent, this parallels to a steady decline of preset temperature control. Figure 17 shows the probability $P(SC|x)$ that the process is still under statistical control over time for different drift values from +0.5 K to

Table 8 Influence of control period on the ranking of possible causes of faults [threshold of 0.6]

Control period δ_c	Probable cause #1	Probable cause #2	Probable cause #3	Probable cause #4	Probable cause #5	Probable cause #6
$\delta_c = 6$ h	IG → 20.2 %	IT → 17.0	Uwa → 13.3	Uwi → 13.0	TB → 10.7	AL → 8.6
$\delta_c = 12$ h	IG → 23.1 %	IT → 16.9	Uwi → 13.2	Uwa → 13.1	TB → 9.2	AL → 7.7
$\delta_c = 24$ h	IT → 29.1 %	IG → 14.0	Uwa → 11.6	Uwi → 11.1	TB → 8.8	AL → 6.8
$\delta_c = 72$ h	IT → 56.1 %	IG → 10.1	Uwi → 7.8	Uwa → 5.2	TB → 4.1	AL → 3.3
$\delta_c = 168$ h	IT → 68.2 %	IG → 6.0	Uwi → 4.9	Uwa → 4.0	TB → 2.4	AL → 1.8

where AL is the air leakage, IT is the indoor or preset temperature, IG is the internal heat gains, Pre is the level of occupancy, Alb is the albedo, GF is the glazing solar factor, GT is the ground temperature, LC is the low ceiling, TB is the thermal bridges, UR isU_{roof} or high ceiling, Uwa is U_{wall}, Uwi is U_{window}, and Ve is the ventilation.

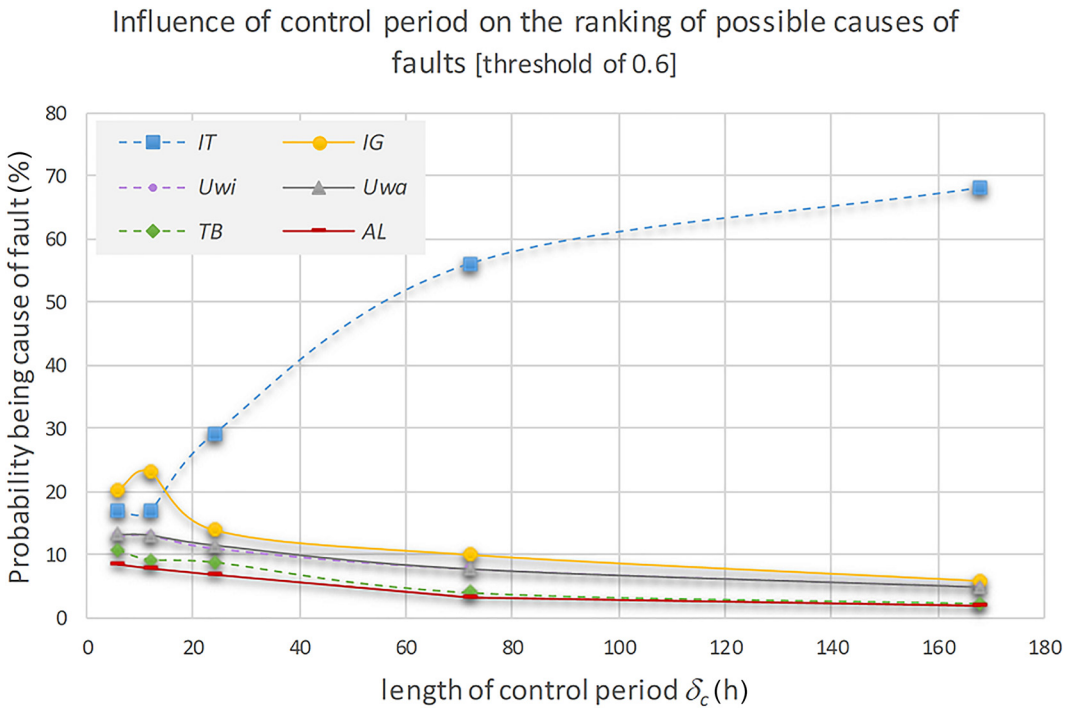

Fig. 19 Simulations of consumption deviations for the case with two simultaneous faults (IT and *Uwi*)

Table 9 Influence of threshold and control period on ranking of possible causes of faults for two faults appearing simultaneously (IT and *Uwi*)

		Control threshold	
		0.75	0.6
Control period	$\delta_c = 48$ h	IT → 32.2%; Uwa → 14.3%; IG → 12.7% Uwi → 11.4%; TB → 7.1%; AL → 5.3%	IT → 40.0; Uwa → 11.4; Uwi → 11.3 IG → 9.8; TB → 5.8; AL → 3.5
	$\delta_c = 144$ h	IT → 37.2; Uwa → 12.6; Uwi → 12.4 IG → 10.7; TB → 6.4; AL → 4.0	IT → 43.6; Uwa → 10.0; Uwi → 9.4 IG → 8.7; TB → 5.0; AL → 3.1

where AL is the air leakage, IT is the indoor or preset temperature, IG is the internal heat gains, Pre is the level of occupancy, Alb is the albedo, GF is the glazing solar factor, GT is the ground temperature, LC is the low ceiling, TB is the thermal bridges, UR isU_{roof} or high ceiling, Uwa is U_{wall}, Uwi is U_{window}, and Ve is the ventilation.

+2 K with a step of 0.5 K. We still consider that, as an example, the detection threshold is 0.6 and the control period is 6 h. We also indicate the different detection times after fault injection (here, fault is arbitrarily injected at 1000 h).

Of course, detection time decreases when the value of drift increases but, as suggested in the previous paragraphs, there is a negative impact on the ability to identify the possible cause leading to the detected fault. The results of simulations presented in Table 6 show this negative impact that will push to focus on the necessary optimization of the control parameters (detection threshold, control period …).

5.3 Influence of Detection Threshold of Control Chart.

The results presented previously (see primarily comments on case_1) suggest that the detection time has an impact on the quality of fault characterization. A short detection time mechanically reduces the quantity of information available to the BN coupled

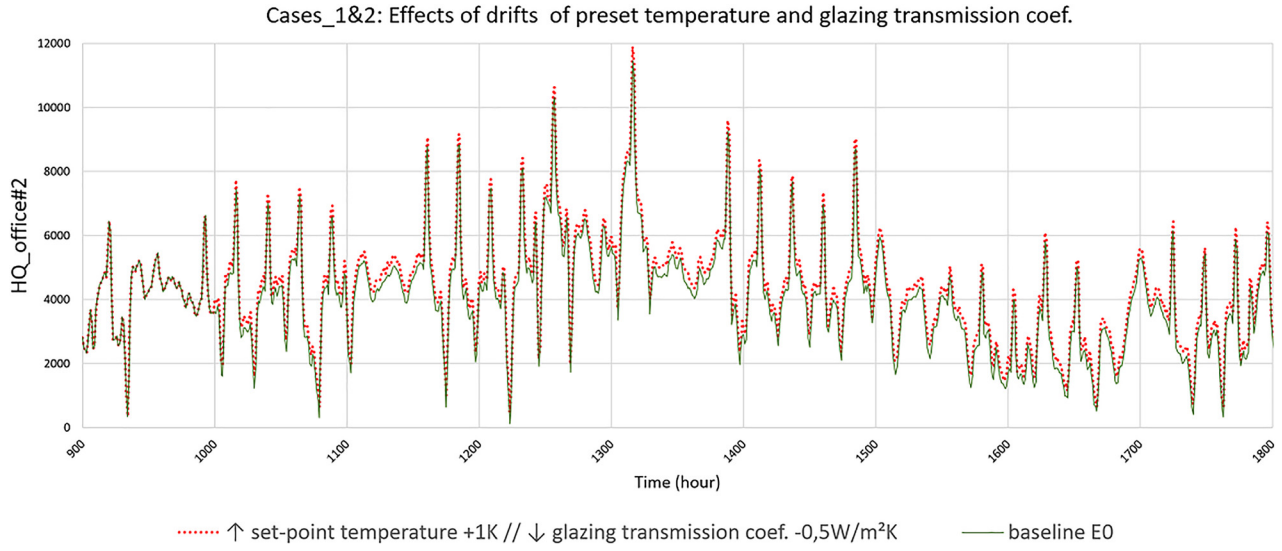

Fig. 20 Simulations of consumption deviations for the case with two simultaneous faults (IT and *Uwi*)

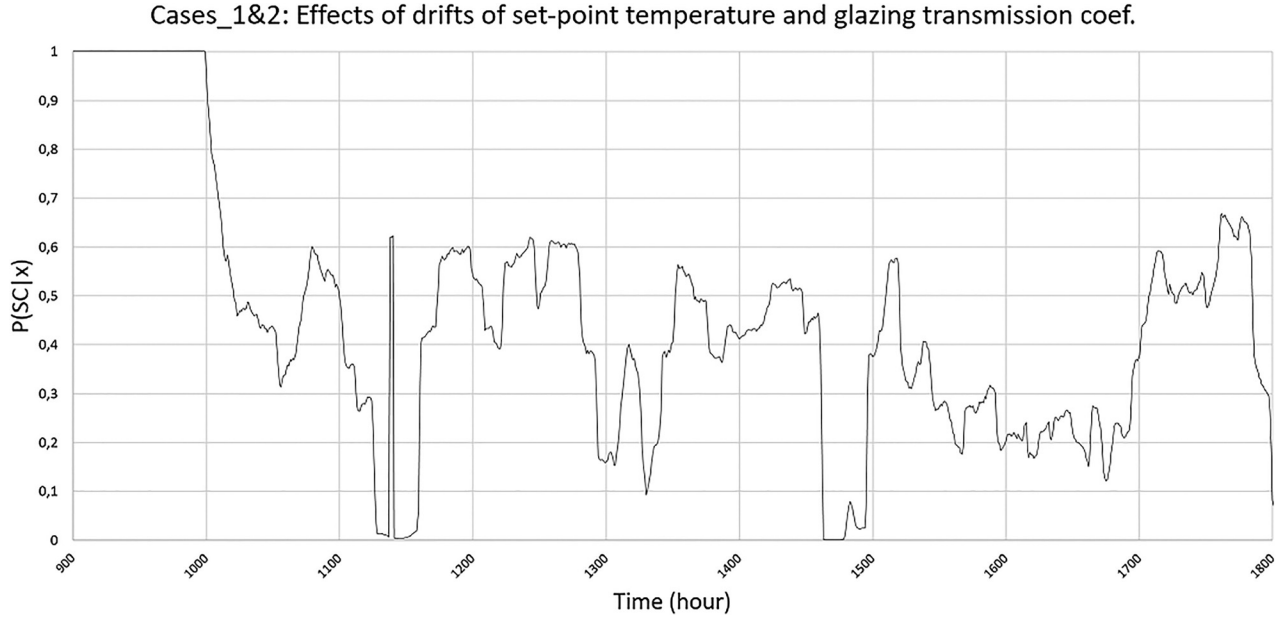

Fig. 21 Probability of process being under SC for a case with two faults appearing simultaneously (IT and *Uwi*)

with control chart, thus increasing the ultimate risk of poor characterization of the fault or drift. This detection time, which we cannot a priori fully control, is linked to the detection threshold of the control chart, which, however, can be controlled/chosen. In Table 7 can be seen the influence of the chosen control chart detection threshold on the characterization of the fault for the first case_1, dealt with previously. The threshold values of 0.6, 0.5, and 0.4 were chosen arbitrarily to illustrate this influence.

We can see that the injected IT fault is identified at the 0.5 threshold (with a corresponding detection time of around 53 h) as the most likely one (and 2.8 times more likely than the second fault, IG). For a threshold value of 0.4 (with a corresponding detection time of roughly 114 h), the first probable cause is unambiguously identified; the probability of the IT fault occurring effectively overtakes that of IG with a ratio of over 15. This high level of discrimination is because the impact of the IT fault alone on consumption deviations is intrinsically far greater than the effects of the other variables.

Finally, we must point out that in the example given in our study the characterization error for low threshold values grows in proportion to the degree to which the first simulated values differ from the mean value calculated between times t_1 and t_2, i.e., the start and end times of the simulation.

5.4 Influence of the Control Period. The previous simulations have demonstrated that modification of the threshold value can improve the characterization of a fault. The aim of adjusting the threshold value in this way is to mechanically increase the duration over which consumption deviations are measured, thus ensuring that comprehensive information is available and used. Another strategy is possible, namely the adjustment of the control period. The idea is that once a fault has been detected, the measurement of deviations continues for a certain time period δ_c in order to obtain a better fault "signature." In practical terms, that means to increase the time duration of the signal analysis, i.e., to insert a time window into the signal (see Fig. 18).

For the threshold of 0.6, which evidently caused problems for the characterization of the fault in simulation case_1, we tested the influence of the control period, i.e., duration δ_c, on the identification of probable causes. Table 8 sums up the results obtained for five values of control period. It shows the impact of the control period on the rank and scale of the probabilities achieved when identifying fault causes. The more the length of the control period δ_c increases, the better the actual cause of fault is detected. In Fig. 19, we show the variation of the probability of being the cause of fault (for the sixth first most probable causes) as a function of δ_c. Factor IT is considered to be the most probable cause of fault as soon as δ_c reaches about 16 h. After 60 h of control period, the probability of factor IT to be the cause of fault is five times higher than the one of the second ranked possible cause of fault. This ratio exceed ten for δ_c beyond 140 h. We might finally be inclined to choose a large control period to be certain to detect the actual cause, but if this control period is too long the consequence of the ongoing deterioration of performance might be too critical. The choice of the control period length is always a matter of compromise (see Table 9).

The results of simulations in Table 9 show that the cause IT is indeed identified as most likely regardless of the control combination (threshold/period). This is primarily due to the fact that fault IT has a greater impact on consumption deviations than do the other variables. As for cause *Uwi*, it does feature among the most likely causes of drift but is never ranked in first or second place, where it should be.

5.5 Influence of Number of Faults. We have demonstrated the rich potential of BNs coupled to a control chart in the presence of a single fault—a potential conditional upon an appropriate degree of adjustment of the thresholds and control period. Here, we examine the appearance, after a period of 1000 h, of two faults simultaneously, on variables IT and *Uwi*. The simulations that we present for office 2 were carried out with two threshold values (0.75 and 0.6) and two control periods (48 and 144 h). Figures 20 and 21 show the results obtained by simulation via BN. Table 9 synthesizes the ranking of probable causes of faults.

In this situation where two faults on IT and *Uwi* are simultaneously injected, we have found that the value of the average relative discrepancy reaches +9.06% with a standard deviation of +7.41%. One remark that the two effects of the fault taken individually are almost added together (we recall that the average discrepancies for case_1 and case_2 have been found, respectively, at +7.64% and 1.86% (see Sec. 5.1)).

6 Conclusion

This paper proposes a hybrid FDD method for detecting faults and energy performance drifts in buildings during its operation and maintenance stage. The method is based on the graphical method of BNs. It is referred as hybrid since we use actual data for the BN construction in functional state and DES to create a complementary database in dysfunctional states. We have shown the potential of the BN in the process of detection and ranking of the probable causes of a fault or drift of energy performance for an actual building located in Les Ponts-de-Cé, France.

Our modeling approach is divided into three stages. In the first one, we compile a whole-year database of hourly measured/actual input variables related to environmental conditions, building envelope and energy systems performances, level of occupancy and outputs (energy needs) extracted from actual data and/or predicted from DES. The DES model of the building is validated by comparisons with the measured energy needs.

In the second stage, we explore a number of alternative Bayesian networks designed for the modeling of a building in operational mode. The BN is used to simulate a baseline of the energy needs variations in this operational mode, as a function of input variables. A robustness study allows us to reduce the size of the database with small disturbances on the BN architecture and on its efficiency. This database reduction and the consequent decrease in the computation time facilitate the development of DBN with continuous nodes for more accurate simulations and better diagnosis and prognostic performances. This DBN is updated in a third stage using DES simulating several types of faults or drifts of the model inputs. Once the inference rules for dysfunctional operating modes are constructed, we carry out FDD simulations. We show the potential but also the limitations of using this approach for the ranking of probable causes of an energy performance fault. Some of these limitations can be explained by imperfect optimization of the control period and the threshold adjustments of the control charts. The suggested approach seems to have a lower degree of accuracy when several faults appear simultaneously. In our further works, we will try to address these shortcomings.

Acknowledgment

This study was funded by the grants from the National Association of Research (ANR) in France within the OMEGA project and the data were provided by CEREMA (Centre d'Etudes et d'expertise sur les Risques, l'Environnement, la Mobilité et l'Aménagement).

Funding Data

- National Association of Research (10.13039/501100001665).

Table 10 The 104 fault situations simulated to update the DBN [low, high, and nominal level of performance are respectively coded by numbers (−1), (+1) and (0)].

Factors →	Air Leakage	Preset temperature	Internal heat Gains	Level of occupancy	Albedo	Glazing solar factor	Ground temperature	Low Ceiling	Thermal Bridges	U_{roof} or high ceiling	U_{wall}	U_{window}	Ventilation
Fault situation # ↓	F1	F2	F3	F4	F5	F6	F7	F8	F9	F10	F11	F12	F13
E1	(+1)	(−1)	(−1)	(−1)	(−1)	(−1)	(−1)	(−1)	(−1)	(−1)	(−1)	(−1)	(−1)
E2	(−1)	(+1)	(−1)	(−1)	(−1)	(−1)	(−1)	(−1)	(−1)	(−1)	(−1)	(−1)	(−1)
E3	(−1)	(−1)	(+1)	(−1)	(−1)	(−1)	(−1)	(−1)	(−1)	(−1)	(−1)	(−1)	(−1)
E4	(−1)	(−1)	(−1)	(+1)	(−1)	(−1)	(−1)	(−1)	(−1)	(−1)	(−1)	(−1)	(−1)
E5	(−1)	(−1)	(−1)	(−1)	(+1)	(−1)	(−1)	(−1)	(−1)	(−1)	(−1)	(−1)	(−1)
E6	(−1)	(−1)	(−1)	(−1)	(−1)	(+1)	(−1)	(−1)	(−1)	(−1)	(−1)	(−1)	(−1)
E7	(−1)	(−1)	(−1)	(−1)	(−1)	(−1)	(+1)	(−1)	(−1)	(−1)	(−1)	(−1)	(−1)
E8	(−1)	(−1)	(−1)	(−1)	(−1)	(−1)	(−1)	(+1)	(−1)	(−1)	(−1)	(−1)	(−1)
E9	(−1)	(−1)	(−1)	(−1)	(−1)	(−1)	(−1)	(−1)	(+1)	(−1)	(−1)	(−1)	(−1)
E10	(−1)	(−1)	(−1)	(−1)	(−1)	(−1)	(−1)	(−1)	(−1)	(+1)	(−1)	(−1)	(−1)
E11	(−1)	(−1)	(−1)	(−1)	(−1)	(−1)	(−1)	(−1)	(−1)	(−1)	(+1)	(−1)	(−1)
E12	(−1)	(−1)	(−1)	(−1)	(−1)	(−1)	(−1)	(−1)	(−1)	(−1)	(−1)	(+1)	(−1)

Table 10 (continued)

Factors →	Air Leakage	Preset temperature	Internal heat Gains	Level of occupancy	Albedo	Glazing solar factor	Ground temperature	Low Ceiling	Thermal Bridges	U_{roof} or high ceiling	U_{wall}	U_{window}	Ventilation
Fault situation # ↓	F1	F2	F3	F4	F5	F6	F7	F8	F9	F10	F11	F12	F13
E13	(−1)	(−1)	(−1)	(−1)	(−1)	(−1)	(−1)	(−1)	(−1)	(−1)	(−1)	(−1)	(+1)
E14	(+1)	(+1)	(−1)	(−1)	(−1)	(−1)	(−1)	(−−1)	(−1)	(−1)	(−1)	(−1)	(−1)
E15	(+1)	(−1)	(+1)	(−1)	(−1)	(−1)	(−1)	(−1)	(−1)	(−1)	(−1)	(−1)	(−1)
E16	(+1)	(−1)	(−1)	(+1)	(−1)	(−1)	(−1)	(−1)	(−1)	(−1)	(−1)	(−1)	(−1)
E17	(+1)	(−1)	(−1)	(−1)	(+1)	(−1)	(−1)	(−1)	(−1)	(−1)	(−1)	(−1)	(−1)
E18	(+1)	(−1)	(−1)	(−1)	(−1)	(+1)	(−1)	(−1)	(−1)	(−1)	(−1)	(−1)	(−1)
E19	(+1)	(−1)	(−1)	(−1)	(−1)	(−1)	(+1)	(−1)	(−1)	(−1)	(−1)	(−1)	(−1)
E20	(+1)	(−1)	(−1)	(−1)	(−1)	(−1)	(−1)	(+1)	(−1)	(−1)	(−1)	(−1)	(−1)
E21	(+1)	(−1)	(−1)	(−1)	(−1)	(−1)	(−1)	(−1)	(+1)	(−1)	(−1)	(−1)	(−1)
E22	(+1)	(−1)	(−1)	(−1)	(−1)	(−1)	(−1)	(−1)	(−1)	(+1)	(−1)	(−1)	(−1)
E23	(+1)	(−1)	(−1)	(−1)	(−1)	(−1)	(−1)	(−1)	(−1)	(−1)	(+1)	(−1)	(−1)
E24	(+1)	(−1)	(−1)	(−1)	(−1)	(−1)	(−1)	(−1)	(−1)	(−1)	(−1)	(+1)	(−1)
E25	(+1)	(−1)	(−1)	(−1)	(−1)	(−1)	(−1)	(−1)	(−1)	(−1)	(−1)	(−1)	(+1)
E26	0	(−1)	(−1)	(−1)	(−1)	(−1)	(−1)	(−1)	(−1)	(−1)	(−1)	(−1)	(−1)
E27	(−1)	0	(−1)	(−1)	(−1)	(−1)	(−1)	(−1)	(−1)	(−1)	(−1)	(−1)	(−1)
E28	(−1)	(−1)	0	(−1)	(−1)	(−1)	(−1)	(−1)	(−1)	(−1)	(−1)	(−1)	(−1)
E29	(−1)	(−1)	(−1)	0	(−1)	(−1)	(−1)	(−1)	(−1)	(−1)	(−1)	(−1)	(−1)
E30	(−1)	(−1)	(−1)	(−1)	0	(−1)	(−1)	(−1)	(−1)	(−1)	(−1)	(−1)	(−1)
E31	(−1)	(−1)	(−1)	(−1)	(−1)	0	(−1)	(−1)	(−1)	(−1)	(−1)	(−1)	(−1)
E32	(−1)	(−1)	(−1)	(−1)	(−1)	(−1)	0	(−1)	(−1)	(−1)	(−1)	(−1)	(−1)
E33	(−1)	(−1)	(−1)	(−1)	(−1)	(−1)	(−1)	0	(−1)	(−1)	(−1)	(−1)	(−1)
E34	(−1)	(−1)	(−1)	(−1)	(−1)	(−1)	(−1)	(−1)	0	(−1)	(−1)	(−1)	(−1)
E35	(−1)	(−1)	(−1)	(−1)	(−1)	(−1)	(−1)	(−1)	(−1)	0	(−1)	(−1)	(−1)
E36	(−1)	(−1)	(−1)	(−1)	(−1)	(−1)	(−1)	(−1)	(−1)	(−1)	0	(−1)	(−1)
E37	(−1)	(−1)	(−1)	(−1)	(−1)	(−1)	(−1)	(−1)	(−1)	(−1)	(−1)	0	(−1)
E38	(−1)	(−1)	(−1)	(−1)	(−1)	(−1)	(−1)	(−1)	(−1)	(−1)	(−1)	(−1)	0
E39	(−1)	(+1)	(+1)	(−1)	(−1)	(−1)	(−1)	(−1)	(−1)	(−1)	(−1)	(−1)	(−1)
E40	(−1)	(+1)	(−1)	(+1)	(−1)	(−1)	(−1)	(−1)	(−1)	(−1)	(−1)	(−1)	(−1)
E41	(−1)	(+1)	(−1)	(−1)	(+1)	(−1)	(−1)	(−1)	(−1)	(−1)	(−1)	(−1)	(−1)
E42	(−1)	(+1)	(−1)	(−1)	(−1)	(+1)	(−1)	(−1)	(−1)	(−1)	(−1)	(−1)	(−1)
E43	(−1)	(+1)	(−1)	(−1)	(−1)	(−1)	(+1)	(−1)	(−1)	(−1)	(−1)	(−1)	(−1)
E44	(−1)	(+1)	(−1)	(−1)	(−1)	(−1)	(−1)	(+1)	(−1)	(−1)	(−1)	(−1)	(−1)
E45	(−1)	(+1)	(−1)	(−1)	(−1)	(−1)	(−1)	(−1)	(+1)	(−1)	(−1)	(−1)	(−1)
E46	(−1)	(+1)	(−1)	(−1)	(−1)	(−1)	(−1)	(−1)	(−1)	(+1)	(−1)	(−1)	(−1)
E47	(−1)	(+1)	(−1)	(−1)	(−1)	(−1)	(−1)	(−1)	(−1)	(−1)	(+1)	(−1)	(−1)
E48	(−1)	(+1)	(−1)	(−1)	(−1)	(−1)	(−1)	(−1)	(−1)	(−1)	(−1)	(+1)	(−1)
E49	(−1)	(+1)	(−1)	(−1)	(−1)	(−1)	(−1)	(−1)	(−1)	(−1)	(−1)	(−1)	(+1)
E50	(−1)	(−1)	(+1)	(+1)	(−1)	(−1)	(−1)	(−1)	(−1)	(−1)	(−1)	(−1)	(−1)
E51	(−1)	(−1)	(+1)	(−1)	(+1)	(−1)	(−1)	(−1)	(−1)	(−1)	(−1)	(−1)	(−1)
E52	(−1)	(−1)	(+1)	(−1)	(−1)	(+1)	(−1)	(−1)	(−1)	(−1)	(−1)	(−1)	(−1)
E53	(−1)	(−1)	(+1)	(−1)	(−1)	(−1)	(+1)	(−1)	(−1)	(−1)	(−1)	(−1)	(−1)
E54	(−1)	(−1)	(+1)	(−1)	(−1)	(−1)	(−1)	(+1)	(−1)	(−1)	(−1)	(−1)	(−1)
E55	(−1)	(−1)	(+1)	(−1)	(−1)	(−1)	(−1)	(−1)	(+1)	(−1)	(−1)	(−1)	(−1)
E56	(−1)	(−1)	(+1)	(−1)	(−1)	(−1)	(−1)	(−1)	(−1)	(+1)	(−1)	(−1)	(−1)
E57	(−1)	(−1)	(+1)	(−1)	(−1)	(−1)	(−1)	(−1)	(−1)	(−1)	(+1)	(−1)	(−1)
E58	(−1)	(−1)	(+1)	(−1)	(−1)	(−1)	(−1)	(−1)	(−1)	(−1)	(−1)	(+1)	(−1)
E59	(−1)	(−1)	(+1)	(−1)	(−1)	(−1)	(−1)	(−1)	(−1)	(−1)	(−1)	(−1)	(+1)
E60	(−1)	(−1)	(−1)	(+1)	(+1)	(−1)	(−1)	(−1)	(−1)	(−1)	(−1)	(−1)	(−1)
E61	(−1)	(−1)	(−1)	(+1)	(−1)	(+1)	(−1)	(−1)	(−1)	(−1)	(−1)	(−1)	(−1)
E62	(−1)	(−1)	(−1)	(+1)	(−1)	(−1)	(+1)	(−1)	(−1)	(−1)	(−1)	(−1)	(−1)
E63	(−1)	(−1)	(−1)	(+1)	(−1)	(−1)	(−1)	(+1)	(−1)	(−1)	(−1)	(−1)	(−1)
E64	(−1)	(−1)	(−1)	(+1)	(−1)	(−1)	(−1)	(−1)	(+1)	(−1)	(−1)	(−1)	(−1)
E65	(−1)	(−1)	(−1)	(+1)	(−1)	(−1)	(−1)	(−1)	(−1)	(+1)	(−1)	(−1)	(−1)
E66	(−1)	(−1)	(−1)	(+1)	(−1)	(−1)	(−1)	(−1)	(−1)	(−1)	(+1)	(−1)	(−1)
E67	(−1)	(−1)	(−1)	(+1)	(−1)	(−1)	(−1)	(−1)	(−1)	(−1)	(−1)	(+1)	(−1)
E68	(−1)	(−1)	(−1)	(+1)	(−1)	(−1)	(−1)	(−1)	(−1)	(−1)	(−1)	(−1)	(+1)
E69	(−1)	(−1)	(−1)	(−1)	(+1)	(+1)	(−1)	(−1)	(−1)	(−1)	(−1)	(−1)	(−1)
E70	(−1)	(−1)	(−1)	(−1)	(+1)	(−1)	(+1)	(−1)	(−1)	(−1)	(−1)	(−1)	(−1)
E71	(−1)	(−1)	(−1)	(−1)	(+1)	(−1)	(−1)	(+1)	(−1)	(−1)	(−1)	(−1)	(−1)
E72	(−1)	(−1)	(−1)	(−1)	(+1)	(−1)	(−1)	(−1)	(+1)	(−1)	(−1)	(−1)	(−1)
E73	(−1)	(−1)	(−1)	(−1)	(+1)	(−1)	(−1)	(−1)	(−1)	(+1)	(−1)	(−1)	(−1)
E74	(−1)	(−1)	(−1)	(−1)	(+1)	(−1)	(−1)	(−1)	(−1)	(−1)	(+1)	(−1)	(−1)
E75	(−1)	(−1)	(−1)	(−1)	(+1)	(−1)	(−1)	(−1)	(−1)	(−1)	(−1)	(+1)	(−1)
E76	(−1)	(−1)	(−1)	(−1)	(+1)	(−1)	(−1)	(−1)	(−1)	(−1)	(−1)	(−1)	(+1)
E77	(−1)	(−1)	(−1)	(−1)	(−1)	(+1)	(+1)	(−1)	(−1)	(−1)	(−1)	(−1)	(−1)
E78	(−1)	(−1)	(−1)	(−1)	(−1)	(+1)	(−1)	(+1)	(−1)	(−1)	(−1)	(−1)	(−1)
E79	(−1)	(−1)	(−1)	(−1)	(−1)	(+1)	(−1)	(−1)	(+1)	(−1)	(−1)	(−1)	(−1)
E80	(−1)	(−1)	(−1)	(−1)	(−1)	(+1)	(−1)	(−1)	(−1)	(+1)	(−1)	(−1)	(−1)

Table 10 (continued)

Factors →	Air Leakage	Preset temperature	Internal heat Gains	Level of occupancy	Albedo	Glazing solar factor	Ground temperature	Low Ceiling	Thermal Bridges	U_{roof} or high ceiling	U_{wall}	U_{window}	Ventilation
Fault situation # ↓	F1	F2	F3	F4	F5	F6	F7	F8	F9	F10	F11	F12	F13
E81	(−1)	(−1)	(−1)	(−1)	(−1)	(+1)	(−1)	(−1)	(−1)	(−1)	(+1)	(−1)	(−1)
E82	(−1)	(−1)	(−1)	(−1)	(−1)	(+1)	(−1)	(−1)	(−1)	(−1)	(−1)	(+1)	(−1)
E83	(−1)	(−1)	(−1)	(−1)	(−1)	(+1)	(−1)	(−1)	(−1)	(−1)	(−1)	(−1)	(+1)
E84	(−1)	(−1)	(−1)	(−1)	(−1)	(−1)	(+1)	(+1)	(−1)	(−1)	(−1)	(−1)	(−1)
E85	(−1)	(−1)	(−1)	(−1)	(−1)	(−1)	(+1)	(−1)	(+1)	(−1)	(−1)	(−1)	(−1)
E86	(−1)	(−1)	(−1)	(−1)	(−1)	(−1)	(+1)	(−1)	(−1)	(+1)	(−1)	(−1)	(−1)
E87	(−1)	(−1)	(−1)	(−1)	(−1)	(−1)	(+1)	(−1)	(−1)	(−1)	(+1)	(−1)	(−1)
E88	(−1)	(−1)	(−1)	(−1)	(−1)	(−1)	(+1)	(−1)	(−1)	(−1)	(−1)	(+1)	(−1)
E89	(−1)	(−1)	(−1)	(−1)	(−1)	(−1)	(+1)	(−1)	(−1)	(−1)	(−1)	(−1)	(+1)
E90	(−1)	(−1)	(−1)	(−1)	(−1)	(−1)	(−1)	(+1)	(+1)	(−1)	(−1)	(−1)	(−1)
E91	(−1)	(−1)	(−1)	(−1)	(−1)	(−1)	(−1)	(+1)	(−1)	(+1)	(−1)	(−1)	(−1)
E92	(−1)	(−1)	(−1)	(−1)	(−1)	(−1)	(−1)	(+1)	(−1)	(−1)	(+1)	(−1)	(−1)
E93	(−1)	(−1)	(−1)	(−1)	(−1)	(−1)	(−1)	(+1)	(−1)	(−1)	(−1)	(+1)	(−1)
E94	(−1)	(−1)	(−1)	(−1)	(−1)	(−1)	(−1)	(+1)	(−1)	(−1)	(−1)	(−1)	(+1)
E95	(−1)	(−1)	(−1)	(−1)	(−1)	(−1)	(−1)	(−1)	(+1)	(+1)	(−1)	(−1)	(−1)
E96	(−1)	(−1)	(−1)	(−1)	(−1)	(−1)	(−1)	(−1)	(+1)	(−1)	(+1)	(−1)	(−1)
E97	(−1)	(−1)	(−1)	(−1)	(−1)	(−1)	(−1)	(−1)	(+1)	(−1)	(−1)	(+1)	(−1)
E98	(−1)	(−1)	(−1)	(−1)	(−1)	(−1)	(−1)	(−1)	(+1)	(−1)	(−1)	(−1)	(+1)
E99	(−1)	(−1)	(−1)	(−1)	(−1)	(−1)	(−1)	(−1)	(−1)	(+1)	(+1)	(−1)	(−1)
E100	(−1)	(−1)	(−1)	(−1)	(−1)	(−1)	(−1)	(−1)	(−1)	(+1)	(−1)	(+1)	(−1)
E101	(−1)	(−1)	(−1)	(−1)	(−1)	(−1)	(−1)	(−1)	(−1)	(+1)	(−1)	(−1)	(+1)
E102	(−1)	(−1)	(−1)	(−1)	(−1)	(−1)	(−1)	(−1)	(−1)	(−1)	(+1)	(+1)	(−1)
E103	(−1)	(−1)	(−1)	(−1)	(−1)	(−1)	(−1)	(−1)	(−1)	(−1)	(+1)	(−1)	(+1)
E104	(−1)	(−1)	(−1)	(−1)	(−1)	(−1)	(−1)	(−1)	(−1)	(−1)	(−1)	(+1)	(+1)

References

[1] de Wilde, P., 2014, "The Gap Between Predicted and Measured Energy Performance of Buildings: A Framework for Investigation," Autom. Constr., **41**, pp. 40–49.

[2] van Dronkelaar, C., Dowson, M., Spataru, C., and Mumovic, D., 2016, "A Review of the Regulatory Energy Performance Gap and Its Underlying Causes in Non-Domestic Buildings," Front. Mech. Eng., **1**(■), ■.

[3] Titikpina, F., Caucheteux, A., Charki, A., and Bigaud, A., 2015, "Uncertainty Assessment in Building Energy Performance With a Simplified Model," Int. J. Metrol. Qual. Eng., **6**(3), p. 308.

[4] Katipamula, S., and Brambley, M. R., 2005, "Review Article: Methods for Fault Detection, Diagnostics, and Prognostics for Building Systems—Part I: A Review," HVACR Res., **11**(1), pp. 3–25.

[5] Jing, R., Wang, M., Zhang, R., Li, N., and Zhao, Y., 2017, "A Study on Energy Performance of 30 Commercial Office Buildings in Hong Kong," Energy Build., **144**, pp. 117–128.

[6] Bynum, J. D., Claridge, D. E., and Curtin, J. M., 2012, "Development and Testing of an Automated Building Commissioning Analysis Tool (ABCAT)," Energy Build., **55**, pp. 607–617.

[7] Wang, L., 2012, "Modeling and Simulation of HVAC Faulty Operations and Performance Degradation Due to Maintenance Issues," Asia Conference of International Building Performance Simulation Association (ASIM'2012), Shangai, China, ■, p. 8.

[8] Verhelst, J., van Ham, G., Saelens, D., and Hensen, L., 2017, "Model Selection for Continuous Commissioning of HVAC-Systems in Office Buildings: A Review," Renewable Sustainable Energy Rev., **76**, pp. 673–686.

[9] Yu, Y. B., Woradechjumroen, D., and Yu, D. H., 2014, "A Review of Fault Detection and Diagnosis Methodologies on Air-Handling Units," Energy Build., **82**, pp. 550–562.

[10] Zhao, Y., Wang, S. W., and Xiao, F., 2013, "A Statistical Fault Detection and Diagnosis Method for Centrifugal Chillers Based on Exponentially-Weighted Moving Average Control Charts and Support Vector Regression," Appl. Therm. Eng., **51**(1–2), pp. 560–572.

[11] Verbert, K., Babuška, R., and De Schutter, B., 2017, "Combining Knowledge and Historical Data for System-Level Fault Diagnosis of HVAC Systems," Eng. Appl. Artif. Intell., **59**, pp. 260–273.

[12] Dong, B., O'Neill, Z., and Li, Z., 2014, "A BIM-Enabled Information Infrastructure for Building Energy Fault Detection and Diagnostics," Autom. Constr., **44**, pp. 197–211.

[13] Wall, J., and Guo, Y., 2018, "RP1026: Evaluation of Next-Generation Automated Fault Detection & Diagnosis (FDD) Tools for Commercial Building Energy Efficiency—Part I: FDD Case Studies in Australia," *Low Carbon Living*, CRC, ■, p. 66.

[14] Abdollahi, A., Pattipati, K. R., Kodali, A., Singh, S., Zhang, S., and Luh, P. B., 2016, "Probabilistic Graphical Models for Fault Diagnosis in Complex Systems," *Principles of Performance Reliability Modeling and Evaluation—Essays in Honor of Kishor Trivedi on His 70th Birthday* (Springer Series in Reliability Engineering), L. Fiondella and A. Puliafito eds., ■, ■, pp. 109–139.

[15] Hao, J., Kang, J., Li, J., and Zhao, Z., 2012, "A Physical Model Based Research for Fault Diagnosis of Gear Crack," International Conference on Quality, Reliability, Risk, Maintenance, and Safety Engineering, Chengdu, China, ■, pp. 572–575.

[16] Schein, J., Bushby, S. T., Castro, N. S., and House, J. M., 2006, "A Rule-Based Fault Detection Method for Air Handling Units," Energy Build., **38**(12), pp. 1485–1492.

[17] Cai, B., Huang, L., and Xie, M., 2017, "Bayesian Networks in Fault Diagnosis," IEEE Trans. Ind. Inf., **13**(5), pp. 2227–2240.

[18] Afram, A., Janabi-Sharifi, F., Fung, A. S., and Raahemifar, K., 2017, "Artificial Neural Network (ANN) Based Model Predictive Control (MPC) and Optimization of HVAC Systems: A State of the Art Review and Case Study of a Residential HVAC System," Energy Build., **141**, pp. 96–113.

[19] Li, G., and Hu, Y., 2019, "An Enhanced PCA-Based Chiller Sensor Fault Detection Method Using Ensemble Empirical Mode Decomposition Based Denoising," Energy Build., **183**, pp. 311–324.

[20] Beghi, A., Cecchinato, L., Corazzol, C., Rampazzo, M., Simmini, F., and Susto, G. A., 2014, "A One-Class SVM Based Tool for Machine Learning Novelty Detection in HVAC Chiller Systems," IFAC Proc. Vol., **47**(3), pp. 1953–1958.

[21] van Every, P. M., Rodriguez, M., Jones, C. B., Mammoli, A. A., and Martínez-Ramón, M., 2017, "Advanced Detection of HVAC Faults Using Unsupervised SVM Novelty Detection and Gaussian Process Models," Energy Build., **149**, pp. 216–224.

[22] He, S., Zhiwei, W., Zhanwei, W., Xiaowei, G., and Zengfeng, Y., 2016, "Fault Detection and Diagnosis of Chiller Using Bayesian Network Classifier With Probabilistic Boundary," Appl. Therm. Eng., **107**(■), pp. 37–47.

[23] Du, Z., and Jin, X., 2008, "Multiple Faults Diagnosis for Sensors in Air Handling Unit Using Fisher Discriminant Analysis," Energy Convers. Manage., **49**(12), pp. 3654–3665.

[24] Kim, W., and Katipamula, S., 2018, "A Review of Fault Detection and Diagnostics Methods for Building Systems," Sci. Technol. Built Environ., **24**(1), pp. 3–21.

[25] Uusitalo, L., 2007, "Advantages and Challenges of Bayesian Networks in Environmental Modelling," Ecol. Modell., **203**(3–4), pp. 312–318.

[26] Taal, A., Itard, L., and Zeiler, W., 2018, "A Reference Architecture for the Integration of Automated Energy Performance Fault Diagnosis Into HVAC Systems," Energy Build., **179**(15), pp. 144–155.

[27] Wang, Z., Wang, Z., Gu, X., He, S., and Yan, Z., 2018, "Feature Selection Based on Bayesian Network for Chiller Fault Diagnosis From the Perspective of Field Applications," Appl. Therm. Eng., **129**(25), pp. 674–683.

[28] Zhao, Y., Wen, J., and Wang, S.-W., 2015, "Diagnostic Bayesian Networks for Diagnosing Air Handling Units Faults—Part II: Faults in Coils and Sensors," Appl. Therm. Eng., **90**(5), pp. 145–157.

[29] Zhao, Y., Wen, J., Xiao, F., Yang, X., and Wang, S.-W., 2017, "Diagnostic Bayesian Networks for Diagnosing Air Handling Units Faults—Part I: Faults in Dampers, Fans, Filters and Sensors," Appl. Therm. Eng., **111**(25), pp. 1272–1286.

[30] Cai, B., Liu, Y., Fan, Q., Zhang, Y., Liu, Z., Yu, S., and Ji, R., 2014, "Multi-Source Information Fusion Based Fault Diagnosis of Ground-Source Heat Pump Using Bayesian Network," Appl. Energy, **114**, pp. 1–9.

[31] Marvin, H. J., Bouzembrak, Y., Janssen, E. M., van der Zande, M., Murphy, F., Sheehan, B., Mullins, M., and Bouwmeester, H., 2017, "Application of Bayesian Networks for Hazard Ranking of Nanomaterials to Support Human Health Risk Assessment," Nanotoxicology, **11**(1), pp. 123–133.

[32] Millán, E., Descalço, L., Castillo, G., Oliveira, P., and Diogo, S., 2013, "Using Bayesian Networks to Improve Knowledge Assessment," Comput. Educ., **60**(1), pp. 436–447.

[33] Shute, V., and Wang, L., 2016, "Assessing and Supporting Hard-to-Measure Constructs in Video Games," *The Wiley Handbook of Cognition and Assessment: Frameworks, Methodologies, and Applications*, ■, ■, pp. 535–562.

[34] Lyons, D. M., Arkin, R. C., Jiang, S., O'Brien, M., Tang, F., and Tang, P., 2017, "Performance Verification for Robot Missions in Uncertain Environments," Rob. Auton. Syst., **98**, pp. 89–104.

[35] Ju, Z., Ji, X., Li, J., and Liu, H., 2017, "An Integrative Framework of Human Hand Gesture Segmentation for Human-Robot Interaction," IEEE Syst. J., **11**(3), pp. 1326–1336.

[36] Slanzi, D., and Poli, I., 2014, "Evolutionary Bayesian Network Design for High Dimensional Experiments," Chemom. Intell. Lab. Syst., **135**(15), pp. 172–182.

[37] Taylor, D., Biedermann, A., Hicks, T., and Champod, C., 2018, "A Template for Constructing Bayesian Networks in Forensic Biology Cases When Considering Activity Level Propositions," Forensic Sci. Int.: Genet., **3**, pp. 136–146.

[38] Szkuta, B., Ballantyne, K. N., Kokshoorn, B., and van Oorscho, R. A. H., 2018, "Transfer and Persistence of Non-Self DNA on Hands Over Time: Using Empirical Data to Evaluate DNA Evidence Given Activity Level Propositions," Forensic Sci. Int.: Genet., **33**, pp. 84–97.

[39] Bae, S.-C., and Lee, Y. H., 2018, "Comparative Efficacy and Tolerability of Monotherapy With Leflunomide or Tacrolimus for the Treatment of Rheumatoid Arthritis: A Bayesian Network Meta-Analysis of Randomized Controlled Trials," Clin. Rheumatol., **37**(2), pp. 323–330.

[40] Chiremsel, Z., Nait Said, R., and Chiremsel, R., 2016, "Probabilistic Fault Diagnosis of Safety Instrumented Systems Based on Fault Tree Analysis and Bayesian Network," J. Failure Anal. Prev., **16**(5), pp. 747–760.

[41] Sousa, H. S., Prieto-Castrillo, F., Matos, J. C., Branco, J. M., and Lourenço, P. B., 2018, "Combination of Expert Decision and Learned Based Bayesian Networks for Multi-Scale Mechanical Analysis of Timber Elements," Expert Syst. Appl., **93**(1), pp. 156–168.

[42] Bishop, C. M., 2006, *Pattern Recognition and Machine Learning*, Springer, ■, p. 738.

[43] Dondelinger, F., Lèbre, S., and Husmeier, D., 2013, "Non-Homogeneous Dynamic Bayesian Networks With Bayesian Regularization for Inferring Gene Regulatory Networks With Gradually Time-Varying Structure," Mach. Learn., **90**(2), pp. 191–230.

[44] Kwisthout, J., 2018, "Approximate Inference in Bayesian Networks: Parameterized Complexity Results," Int. J. Approximate Reasoning, **93**, pp. 119–131.

[45] Wu, P. P.-Y., Julian Caley, M., Kendrick, G. A., McMahon, K., and Mengersen, K., 2018, "Dynamic Bayesian Network Inferencing for Non-Homogeneous Complex Systems," J. R. Stat. Soc. Ser. C: Appl. Stat., **67**(2), pp. 417–434.

[46] Black, A., Korb, K. B., and Nicholson, A. E., 2014, "Intrinsic Learning of Dynamic Bayesian Networks," *PRICAI 2014: Trends in Artificial Intelligence* (Lecture Notes in Computer Science), Vol. 8862, ■, ■, pp. 256–269.

[47] Hu, M., Chen, H., Shen, L., Li, G., Guo, Y., Li, H., Li, J., and Hu, W., 2018, "A Machine Learning Bayesian Network for Refrigerant Charge Faults of Variable Refrigerant Flow Air Conditioning System," Energy Build., **158**, pp. 668–676.

[48] Lin, S., Chen, X., and Wang, Q., 2018, "Fault Diagnosis Model Based on Bayesian Network Considering Information Uncertainty and Its Application in Traction Power Supply System," IEEJ Trans. Electr. Electron. Eng., **13**(5), pp. 671–680.

[49] Verron, S., 2007, "Diagnosis and Monitoring of Complex Processes Via Bayesian Networks," Ph.D. thesis, University of Angers, Angers, France.

[50] Pillet, M., Boukar, A., Pairel, E., Rizzon, B., Boudaoud, N., and Cherfi, Z., 2013, "Multivariate SPC for Total Inertial Tolerancing," Int. J. Metrol. Qual. Eng., **4**(3), pp. 169–175.

[51] Caucheteux, A., Sabar, A. E., and Boucher, V., 2013, "Occupancy Measurement in Building: A Literature Review, Application on an Energy Efficiency Research Demonstration Building," Int. J. Metrol. Qual. Eng., **4**(2), pp. 135–144.

[52] ASHRAE Guideline 14—American Society of Heating, Refrigeration and Air Conditioning Engineers, 2014, "ASHRAE Guideline 14 for Measurement of Energy and Demand Savings," Atlanta, GA.

[53] EVO—Efficiency Valuation Organization, 2012, "International Performance Measurement and Verification Protocol: Concepts and Options for Determining Energy and Water Savings," ■, ■, Report No. EVO 10000 – 1:2012.

[54] WMO, 2008, *Guide to Meteorological Instruments and Methods of Observation*, 7th ed., Word Meteorological Organization, Geneva, Switzerland.

[55] ASHRAE—American Society of Heating, Refrigeration and Air Conditioning Engineers, 2017, "Thermal Environmental Conditions for Human Occupancy," ASHRAE, Atlanta, GA, Standard No. 55.

[56] Caucheteux, A., Gautier, A., and Lahrech, R., 2016, "A Metamodel-Based Methodology for an Energy Savings Uncertainty Assessment of Building Retrofitting," Int. J. Metrol. Qual. Eng., **7**(4), p. 402.

[57] Calì, D., Matthes, P., Huchtemann, K., Streblow, R., and Müller, D., 2015, "CO2 Based Occupancy Detection Algorithm: Experimental Analysis and Validation for Office and Residential Buildings," Building Environ., **86**, pp. 39–49.

[58] Ansanay-Alex, G., Abdelouadoud, Y., and Schetelat, P., 2016, "Statistical and Stochastic Modelling of French Households and Their Energy Consuming Activities," 12th REHVA World Congress-CLIMA, ■, ■, ■.

[59] Yan, D., O'Brien, W., Hong, T., Feng, X., Gunay, H. B., Tahmasebi, F., and Mahdavi, A., 2015, "Occupant Behavior Modeling for Building Performance Simulation: Current State and Future Challenges," Energy Build., **107**, pp. 264–278.

[60] Murphy, K., 2001, "The Bayesian Network Toolbox for Matlab," ■, ■, ■, https://www.cs.ubc.ca/~murphyk/Papers/bnt.pdf

[61] Lauritzen, S. L., 1992, "Propagation of Probabilities, Means and Variances in Mixed Graphical Association Models," J. Am. Stat. Assoc., **87**(420), pp. 1098–1108.

[62] Lauritzen, S. L., and Jensen, F., 2001, "Stable Local Computation With Conditional Gaussian Distributions," Stat. Comput., **11**(2), pp. 191–203.

[63] Sachs, K., Perez, O., Pe'er, D., Lauffenburger, D. A., and Nolan, G. P., 2005, "Causal Protein-Signaling Networks Derived From Multiparameter Single-Cell Data," Science, **308**(5721), pp. 523–529.

[64] Claeskens, G., and Hjort, N. L., 2008, *Model Selection and Model Averaging* (Part of Cambridge Series in Statistical and Probabilistic Mathematics), Cambridge Press, Cambridge, UK, p. 332.

[65] Ghahramani, Z., 2001, "An Introduction to Hidden Markov Models and Bayesian Networks," Int. J. Pattern Recognit. Artif. Intell., **15**(1), pp. 9–42.

[66] Vlachopoulou, M., Chin, G., Fulle, J., and Lu, S., 2014, "Aggregated Residential Load Modeling Using Dynamic Bayesian Networks," IEEE International Conference on Smart Grid Communications, SmartGridComm, ■, ■, pp. 818–823.

[67] Ghahramani, A., Tang, C., Yang, Z., and Becerik-Gerber, B., 2015, "A Study of Time-Dependent Variations in Personal Thermal Comfort Via a Dynamic Bayesian Network," First International Symposium on Sustainable Human-Building Ecosystems, Pittsburgh, PA, Oct. 5–6, 2015, pp. 99–107.

[68] Markovic, R., Wolf, S., Cao, J., Spinnräker, E., Wölki, D., Frisch, J., and van Treeck, C., 2017, "Comparison of Different Classification Algorithms for the Detection of User's Interaction With Windows in Office Buildings," International Conference on Future Buildings and Districts—Energy Efficiency From Nano to Urban Scale (CISBAT), Lausanne, Switzerland, Sept. 6–8, pp. 337–342.

[69] Cai, B., Liu, Y., Ma, Y., Huang, L., and Liu, Z., 2015, "A Framework for the Reliability Evaluation of Grid-Connected Photovoltaic Systems in the Presence of Intermittent Faults," Energy, **93**, pp. 1308–1320.

[70] Hastie, T., Efron, B., 2012, "Lars: Least Angle Regression, Lasso and Forward Stage Wise. R Package Version 1.1," ■, ■.

AQ10 AQ11 AQ12 AQ13